Magnetic properties of galaxies deficient in gas and weakly forming stars

Marek Weżgowiec

PhD Thesis in Astronomy
made at the Faculty of Physics,
Astronomy and Applied Computer Science
of the Jagiellonian University
under the supervision of
Prof. dr hab. Marek Urbanik

Kraków 2009

Acknowledgements

To my family and to all those who made me be at this point.

Abstract

Spiral galaxies are known to have gaseous disk abundant in neutral hydrogen what is the main cause for these objects to form stars at a significant rate. There are however many spiral galaxies, which due to various phenomena have its gaseous content degraded or form stars less rapidly than normal spirals. They may have star formation even completely ceased. The reason for that is likely the influence exerted by a group or a cluster environment, abundant in galaxies, in which tidal or ram-pressure stripping interactions are common. As a result, spiral galaxies existing in a cluster environment are susceptible to the action of such effects and in consequence may be partially devoid of the gaseous component, which can lead to weakening of their magnetic fields. This thesis presents a selected sample of Virgo Cluster spiral galaxies showing low-to-moderate abundance of the interstellar medium. The study involved the radio polarization and X-ray observations. Total power and polarized intensity radio maps are presented together with derived Faraday rotation distributions (where possible). Based on these observations magnetic field strengths for each galaxy are calculated. Maps of the extended emission from the hot gas visible in X-ray band are discussed as well. For most sensitive X-ray observations spectral analysis of the hot gas was performed to study its characteristics. Together with radio polarimetry it provides a good possibility to examine different phenomena that lead to gas deficiency and slow down the star-formation activity in spiral galaxies. This can help to determine their impact on magnetic fields of perturbed galaxies.

Contents

List of Tables

List of Figures

Chapter 1

Introduction

It is known that galaxies are sources of radio emission. In case of early-type galaxies most of this emission comes from their central parts associated with the nuclear region. All of the gaseous matter have been already transformed into the stars. Late-type galaxies, however, still possess significant amounts of the interstellar medium (ISM), which consists of neutral or ionized hydrogen, as well as cold molecular clouds. The existence of these, under favourable conditions, would allow to start star formation. This in turn would lead to an efficient enrichment of the interstellar medium, as it eventually causes the rise of the number of supernovae explosions. Supernovae remnants contribute to the ISM with large amounts of cosmic rays. Cosmic ray electrons moving in the magnetic field of the galaxy emit electromagnetic radiation which provides us with a valuable information about the magnetic field itself, as well as about the general conditions occuring in the galactic disk. It is obvious that the intensity of the radio emission is directly connected to the strength of the magnetic field, as well as to the star forming activity of the galaxy. In the regions of the galaxy with a high star formation level more intense radio emission is observed (Chyży et al. 2007). However, a turbulent magnetic field is present there, as it is known to be frozen into the turbulent matter. If we come across regions of less turbulent medium, there is a high possibility that the observed magnetic fields will be more regular (Chyży et al. 2007). This will manifest in a stronger polarized intensity emitted by electrons moving in such fields. The strength of the signal, as well as its ratio to the total radio intensity (the degree of polarization) will tell us about the degree of ordering of the magnetic field.

Since the magnetic field is co-existing with the ISM (i.e. only with the presence of cosmic rays we have the possibility of observing the magnetic fields via synchrotron emission) it is possible to investigate how it behaves when the ISM distribution is distorted. The interstellar medium can be influenced by various phenomena, which result in compressions, formation of outflow tails or even (at least partial) removal of the gas. We would expect such phenomena to have also effects upon properties of the magnetic field, especially its strengths and the structure of its components.

The main two groups of phenomena are gas deficiences and gas compressions. In both cases a major role is played by interaction effects. They can be of tidal nature (see Toomre & Toomre 1972), when two or more galaxies interact gravitationally – this seems to happen quite often in denser environments such as groups or clusters of galaxies – or due to the so-called ram-pressure stripping, first discussed by Gunn & Gott (1972). The latter is an interaction of a rapidly moving galaxy with the surrounding hot intracluster medium (ICM), during which the outer parts of the gaseous disk of galaxies can be truncated or even totally removed. The outcome of such process is a significant deficiency of neutral hydrogen in the galactic disk (Cayatte et al. 1990, 1994). However, the action of ram-pressure sometimes may cause disk distortions, which may lead to gas compression. Such an outcome of the action of ram-pressure effects was described by Vollmer (2001). Significant compression can trigger star formation in the regions where the ISM density has risen and also amplify the magnetic field causing its higher ordering in the compression area. It is worth noticing that in case of ram-pressure stripping effects only the diffuse gas component is affected (Chemin et al. 2006), while tidal interactions obviously influence both gaseous and stellar content of a galaxy. Although such interactions require well determined conditions, they seem to be quite common in denser groups or in the cluster environment, where the relative distances between galaxies are of an order of magnitude smaller than for field objects. Tidal interactions can cause ISM and magnetic field compressions, as well as gas exchange between interacting galaxies. This is the case of NGC 4254, where one of the spiral arms have been tidally stretched by a perturbing companion, what produced a ridge of higher radio polarized emission (Chyży et al. 2007). Also the infall of gas from the companion galaxy was suggested.

As compressions of the ISM and/or magnetic field obviously cause enhancements in star formation or magnetic fields, it is highly interesting to study the magnetic properties of the galaxies deficient in gas, where star formation activity is suppressed. This way we can find whether magnetic field strength significantly differs from those in normal spiral galaxies. What is the contribution of interaction effects to the global structure of the magnetic field in such galaxies would be another important question.

The main aim of this work is to study magnetic field structures in galaxies with rather low star formation rate and/or with lower ISM content. Such objects can be found in galaxy clusters because of the reasons mentioned above. For these reasons we have selected spiral galaxies, which are members of the Virgo Cluster. A brief description of this cluster together with an explanation of the choice scheme will be presented in Sect. 2.1.1.

Since our studies focus on magnetic fields we make use of the radio polarimetry (see Sect. 1.1), which proved to be a very useful and sensitive tool in tracing any distortions of the magnetic structure of disk spiral galaxies (Soida et al. 1996, Chyży et al. 2002 and 2008).

To make the investigations more comprehensive we also performed an analysis of the X-ray data for selected galaxies. In two cases we performed sensitive observations using XMM-Newton Space Telescope (Jansen et al. 2001) and for the remaining galaxies we searched the XMM-Newton Science Archive (see Sect. 2.3). The X-ray data analysis allowed a comparison of the distribution of hot interstellar gas with the structure of magnetic fields. A spectral analysis, where possible, may help to determine physical conditions and the origin of X-ray emitting gas, hence the nature of possible interactions.

In the next sections of this Chapter, a brief account on radio polarimetry and X-ray observations will be given, as well as a description of the Virgo Cluster in terms of studied galaxies. Chapter 2 contains detailed description of performed observations, both radio and X-ray, as well as the main methods of data reduction, including the archive data. All results are presented in Chapter 3, and its discussion and interpretation in Chapter 4. Chapter 5 summarizes the conclusions of this thesis.

1.1 Radio Polarimetry

As it was mentioned above, by observing the radio polarized intensity we can obtain information about the regular magnetic fields. The stronger the polarized intensity and the higher the degree of polarization, the more ordered is the magnetic field. It is often observed in the position of compressions of the ISM. On the other hand, low gas density ρ leads to lower star formation according to the *Schmidt law* SFR $\propto \rho^n$, where $n \simeq 1.5$ (Wong & Blitz 2002), which in turn causes the ISM to be less turbulent. Therefore, despite overall lower radio emission we might have better opportunities to observe more ordered magnetic fields in gas deficient galaxies.

The interactions between the interstellar medium of the galaxies and the ICM are already known to cause strong gas compression effects, observed as H I ridges in the outskirts of galactic disks (Cayatte et al. 1990). Observations of the polarized radio continuum emission in perturbed galaxies are known to constitute a sensitive way to trace the peculiar gas motions and compression effects even when the disturbances are almost impossible to detect in other domains (Soida et al. 2001). For cluster galaxies it is also possible to guess the directions of the gas flows in the sky plane, adding another dimension to the radial velocity studies (Urbanik 2005).

Observations of the polarized intensity provides us with the information about the sky-plane component of the magnetic field. The observed polarization angle will directly tell us about the magnetic field geometry, provided the frequency of the observations will be high enough to avoid significant Faraday effects. These effects result in depolarization, which is caused by the rotation of the polarization angle of the radiation moving through the magneto-ionic medium. The amount of the rotation depends on the observation frequency and is proportional to λ^2. Nevertheless, single frequency observations will provide only information about the ordering of the magnetic field. Observations at different frequencies allow us to measure the Faraday rotation effect, which makes possible to obtain information about the magnetic field component parallel to the line of sight. Rotation measure (RM) data allows to discriminate between pseudo-regular (ordered but incoherent) and regular (ordered and coherent) magnetic field, as only the regular magnetic field would show large-scale structure in the RM maps, while in an incoherent (or pseudo-regular) field RMs are random and show no large-scale structure (see e.g. Beck 2001). Therefore, multi-frequency observations of the radio polarized intensity can give us clues about the global morphology of the magnetic field of the observed galaxy.

In the case of studying the ISM perturbations, which sometimes are very weak and cause only weakly visible effects, the sensitivity plays the most crucial role. We use a single-dish antenna, as very often high resolution observations provide detailed and accurate data, but obscure the global structure at the same time. A small beam does not allow to observe large areas of diffuse emission, especially those with a low surface-brightness, which is of most importance in tracing global structures of magnetic fields in diffuse ISM of galaxies. Furthermore, sometimes significant amounts of the flux (even up to 30%) can be lost due to a missing zero spacing problem occuring in the observations with the use of an interferometric system. For these reasons, we use the 100-m Effelsberg radio telescope. Large beams of the telescope (e.g. $1\farcm5$ and $2\farcm5$ at 8.35 GHz and 4.85 GHz, respectively) are rather an advantage in our case, as they provide, together with a large collecting area (only 1.7 times smaller than that of the VLA), a very high sensitivity to diffuse extended structures. Such a choice is additionally supported by the fact that this study concentrates on galaxies deficient is gas or slowly forming stars, which are expected to have lower overall radio emission.

1.2 Soft X-ray extended emission studies

In most cases the gas deficiency in galaxies can be caused by interactions with the environment, during which substantial amounts of the ISM can be blown outside of the galaxy in the course of ram-pressure stripping or pulled out during strong tidal encounter. Such ISM removal can be also caused by a starburst phase in the galactic evolution. In either case we can expect to find some leftover emission from the hot gas produced by previous activity like interactions of the ISM with hot ICM or rapid star formation resulting in frequent supernovae explosions. Such emission manifest itself most distinctly in the X-ray band of 0.2 - 1 keV. We can thus perform sensitive observations to study the distribution of the hot gas and its spectral properties which may yield information about the evolution of the ISM of the galaxy, hence the history of the galaxy itself. The spectral analysis however depends on the sensitivity of the acquired data. Using suitable filter and performing long observations under a good cosmic weather conditions (see Sect. 2.3), we may obtain sufficient count rates which will allow us the detailed analysis of the X-ray emission. Fitting a model to such data will provide us with such parameters as the gas temperature, electron density or even metalicities, provided the data are sensitive enough. All this can put important constraints on the conclusions drawn from our radio polarized intensity studies. Detailed properties of the hot gas can be acquired, which together with radio data would help to discriminate between possible scenarios of the origin of the medium and its distortions.

Chapter 2

Observations and Data Reduction

2.1 Selection of the sample

2.1.1 The Virgo Cluster

Considering the characteristics presented in Sect. 1 and required for our target objects, we observed spiral galaxies in the Virgo Cluster. The main advantage is the proximity of this cluster. It is the nearest cluster of galaxies, situated at the distance of only 17 Mpc[1]. This enables a sufficient resolution of the observations with 100-m Effelsberg radio telescope, reaching 12.5 kpc at 4.85 GHz and 7.5 kpc at 8.35 GHz at the assumed distance to the Virgo Cluster. Bearing in mind that the highest possible sensitivity to extended structures was the major goal, we can assume that this makes the best compromise between resolution and sensitivity to study the global magnetic fields of the observed galaxies.

Another good reason for choosing this cluster is its morphology. It has an irregular structure, with a large amount of spiral galaxies, as it is a young dynamically active system being still formed. This means that we can observe strong and frequent interactions between galaxies or within the system as a whole (i.e. ram-pressure stripping). As the intensity of such interations may vary significantly across the cluster, due to different ICM density or galactic velocities, we may expect their different influence upon the distribution of the ISM of galaxies. The main subcluster is concentrated around M 87 and is found to be abundant in a high density ICM as seen in X-ray maps of Böhringer et al. (1994). The southern extension of the cluster forms another

[1]We use a Hubble constant of $H_0 = 70\ \mathrm{km\,s^{-1}\,Mpc^{-1}}$.

subcluster concentrated around the giant elliptical galaxy M49. It is smaller, less dense, though associated with another distinct concentration of the hot gas.

2.1.2 The Sample of Galaxies

Two characteristics, moderate-to-low star formation level and/or gas deficiency of the chosen galaxies played crucial role. The selection of these parameters was based on the Hα and H I studies of Cayatte et al. (1994), Gavazzi et al. (2005), Koopmann et al. (2001, 2004) and Chung et al. (2007). To make our study of the magnetic properties comprehensive, we studied galaxies with various degree of gas deficiency, as well as different origin of this deficiency resulting from various kinds of interactions within the Virgo Cluster. The following galaxies were chosen:

- NGC 4298 and NGC 4302 - mildly gas deficient galaxies possibly interacting in the cluster outskirts.
- NGC 4321 - a barred galaxy with a moderate gas deficiency, without any distinct signs of interactions.
- NGC 4388 - a heavily stripped galaxy in the cluster core.
- NGC 4438 - heavily distorted galaxy interacting with a companion galaxy NGC 4435 in the cluster core, showing unusual Hα bridge towards the giant elliptical M 86 (Kenney et al. 2008).
- NGC 4501 - fast moving galaxy in the mid distance from the cluster centre with a compression visible even in the optical images.
- NGC 4535 - a symmetric barred galaxy with a moderate gas deficiency located in the southern outskirts of the cluster.
- NGC 4548 - an extremely anaemic galaxy located at the moderate distance from the cluster centre.
- NGC 4569 - an anaemic galaxy with unusual radio lobes found by Chyży et al. (2006).

For completeness of this study we included NGC 4254, the galaxy suggested to be tidally interacting (Phookun et al. 1993, Chyży et al. 2007, Minchin et al. 2007) but showing no decrease neither in the star formation level nor its gas content. This allows us to study magnetic properties in a wide range of gas abundance and star-formation activity. The radio data of NGC 4254, as well as those for NGC 4569 together with a detailed discussion was presented by Soida et al. (1996) and Chyży et al. (2006, 2007 and 2008). Therefore, this thesis will present only X-ray data for these galaxies, however, major conclusions drawn from the radio data will also be cited.

2.2 Radio maps

The radio observations were performed between March 2001 and May 2003 (NGC 4438, NGC 4501, NGC 4535, NGC 4548) and between August 2005 and May 2006 (NGC 4298 with NGC 4302, NGC 4321, NGC 4388 and again NGC 4535) using the 100-m Effelsberg radio telescope of the Max-Planck-Institut für Radioastronomie[2] (MPIfR) in Bonn. The basic astronomical properties of the observed objects are summarized in Table 2.1. The above radio observations were performed in collaboration with M. Urbanik, K. T. Chyży and M. Soida from the Obserwatorium Astronomiczne Uniwersytetu Jagiellońskiego in Kraków, Poland, R. Beck from the Max-Planck-Institut für Astronomie in Bonn, Germany, B. Vollmer from the CDS, Observatoire Astronomique de Strasbourg in Strasbourg, France and Ch. Balkowski from the Observatoire de Paris in Paris, France.

All galaxies were observed at 4.85 GHz using the two-horn system (with horn separation of $8'$) in the secondary focus of the radio telescope (see Gioia et al. 1982). NGC 4298 with NGC 4302, NGC 4321, and NGC 4535 were additionally observed at 8.35 GHz using the single horn receiver while NGC 4501 was observed at 10.45 GHz with a four-horn system (Schmidt et al. 1993). Each horn was equipped with two total power receivers and an IF polarimeter resulting in 4 channels containing the Stokes parameters I (2 channels), Q and U. The telescope pointing was corrected every 1.5 hour by performing cross-scans of a bright point source close to the observed galaxy. The flux density scale was established by mapping point sources 3C 138 and 3C 286.

The data reduction was performed using the NOD2 data reduction package (Haslam 1974). At 8.35 GHz (single horn) we performed scans alternatively along the R.A. and Dec. directions. At 4.85 GHz and at 10.45 GHz (dual or multibeam systems used) a number of coverages in the azimuth-elevation frame were obtained for each galaxy, as indicated in Table 2.2. By combining the information from appropriate horns, using the "software beam-switching" technique (Morsi & Reich 1986) followed by a restoration of total intensities (Emerson et al. 1979), we obtained for each coverage the

[2] http://www.mpifr-bonn.mpg.de

Table 2.1: Basic astronomical properties of studied galaxies

NGC	Morph. type[a]	Optical position[a] α_{2000}	δ_{2000}	Incl.[a] [°]	Pos. ang.[a][°]	Proj. dist. to Vir A [°]
4254	Sc	$12^h18^m49\overset{s}{.}6$	$+14°24'59''$	32	60	3.56
4298	Sc	$12^h21^m32\overset{s}{.}8$	$+14°36'22''$	56	135.7	3.14
4302	Sc	$12^h21^m42\overset{s}{.}5$	$+14°35'52''$	90	177.5	3.12
4321	SABb	$12^h22^m55\overset{s}{.}0$	$+15°49'21''$	30	130	3.9
4388	Sb	$12^h25^m46\overset{s}{.}8$	$+12°39'44''$	82	91.3	1.26
4438	Sa	$12^h27^m45\overset{s}{.}9$	$+13°00'32''$	90	27	0.9
4501	Sb	$12^h31^m59\overset{s}{.}3$	$+14°25'14''$	60	138	2
4535	SBc	$12^h34^m20\overset{s}{.}4$	$+08°11'52''$	41.3	180	4.3
4548	SBb	$12^h35^m26\overset{s}{.}4$	$+14°29'47''$	35	150	2.4
4569	SABa	$12^h36^m50\overset{s}{.}1$	$+13°09'46''$	66	23	1.66

[a] taken from HYPERLEDA database – http://leda.univ-lyon1.fr – see Paturel et al. (2003).

I, Q, and U maps of the galaxy. The maps were then combined using the spatial-frequency weighting method (Emerson & Gräve 1988) followed by a digital filtering process, that removed the spatial frequencies corresponding to noisy structures smaller than the telescope beam. Next, we obtained the final maps of total power, polarized intensity, polarization degree and polarization position angles using the AIPS package.

To show the structure of the magnetic field projected to the sky plane we use apparent polarization B-vectors defined as E-vectors rotated by 90°. It is a good approximation of the sky-projected orientation of large scale regular magnetic fields. Possible Faraday rotation bias reaches some ±10° at 8.35 GHz and ±23° at 4.85 GHz in the regions of significant polarized intensity emission in which RM reaches values of ±110 rad/m^2 (see Chapter 3). For each galaxy we present highest resolution data available and in the case of NGC 4535 we present also lower resolution data, as this galaxy shows overall low radio emission.

Table 2.2: Parameters of radio observations of studied galaxies

NGC	Number of coverages	r.m.s in final TP map [mJy/b.a.]	r.m.s in final PI map [mJy/b.a.]
4302*	18[c]	0.3[c]	0.07[c]
	11[b]	0.8[b]	0.08[b]
4321	21[c]	0.3[c]	0.07[c]
	15[b]	0.8[b]	0.1[b]
4388	12[b]	0.9[b]	0.1[b]
4438	25[b]	0.7[b]	0.07[b]
4501	12[d]	0.9[b]	0.09[b]
	23[d]	0.4[d]	0.17[d]
4535	20[c]	0.3[c]	0.07[c]
	10[b]	0.7[b]	0.1[b]
4548	11[b]	0.8[b]	0.09[b]

* Together with NGC 4298.
[a] taken from HYPERLEDA database – http://leda.univ-lyon1.fr – see Paturel et al. (2003).
[b] at 4.85 GHz.
[c] at 8.35 GHz.
[d] at 10.45 GHz.

2.3 X-ray soft extended emission

2.3.1 Our observations

The observations of NGC 4254 and NGC 4569 using XMM-Newton Space Telescope were performed on 29th June 2003 and 13/14th December 2004, respectively. The observations of NGC 4254 were performed in collaboration with M. Ehle from ESAC, XMM-Newton Science Operations Centre in Madrid, Spain, M. Urbanik, K. T. Chyży and M. Soida from the Obserwatorium Astronomiczne Uniwersytetu Jagiellońskiego in Kraków, Poland, W. Pietsch from the Max-Planck-Institut für extraterrestrische Physik in Garching, Germany and Jonathan Braine from the Universite de Bordeaux in Floirac, France. The observations of NGC 4569 were performed in collaboration with M. Ehle from ESAC, XMM-Newton Science Operations Centre in Madrid, Spain, M. Urbanik, K. T. Chyży and M. Soida from the Obserwatorium Astronomiczne Uniwersytetu Jagiellońskiego in Kraków, Poland, D. J. Bomans from the Astronomisches Institut der Ruhr-Universität Bochum in Bochum, Germany and B. Vollmer from the CDS, Observatoire Astronomique de Strasbourg in Strasbourg, France.

To fully meet the need for sensitive observations that would allow the detailed investigation of diffuse soft X-ray emission, long observations using thin filter were performed (see Table 2.3). In case of observations of NGC 4569 a good cosmic weather provided good quality data, which were carefull screened for high energy proton flaring. For the second object, NGC 4254, long periods of high flaring background resulted in significant reduction of the observational time possible to use. In this case, however, the data are sufficient for the spectral analysis due to high X-ray luminosity of this galaxy, which provided enough counts.

2.3.2 Archive data

For the remaining galaxies, except NGC 4548 and NGC 4535, we used public data from the XMM-Newton Science Archive. In case of NGC 4388 and NGC 4438 only off-axis observations were possible to obtain (observations of other sources). For most sources the observing time seemed to be long enough for our purposes to perform the spectral analysis. However, after screening of the data, large parts of the observations needed to be excluded. In two cases (NGC 4298/NGC 4302 and NGC 4438), it was possible to further process the data. For each galaxy it was possible to produce images in the soft band which allowed at least partial analysis of gas distribution. The summary of observations is presented in Table 2.3.

2.3.3 Data reduction

The data was processed using the SAS 8.0 package (Gabriel et al. 2004) with standard reduction procedures. Following the routine of tasks *epchain* and *emchain* event lists for two MOS cameras (Turner et al. 2001) and pn camera (Strüder et al. 2001) for each galaxy were obtained. Next, the event lists were carefully filtered for bad CCD pixels and periods of intense radiation of high energy background. The filtered event lists were used to produce images, background images, exposure maps (without and with vignetting correction), masked for an acceptable detector area using the images script[3]. All images and maps were produced in the band of 0.2 - 1 keV. Next, the final images were combined using the data from all cameras. The resulting images were smoothed with a Gaussian beam of $10''$ HPBW. To get a better signal to noise ratio and thus better sensitivity for extended structures, as well as in order to remove from the final images any distortions caused by the gaps between instrument detectors, the images were again smoothed, this time with a Gaussian beam of $30''$ using the AIPS package. This was also done to allow a better comparison with the radio maps. For NGC 4254, NGC 4298/NGC 4302, NGC 4438 and NGC 4569, where the data was sensitive enough, spectral analysis was performed. For creating spectra only the data from pn camera was used. Event lists were searched for the background point sources using the standard SAS *edetect_chain* procedure. Next, for the relevant regions of each galaxy a spectrum was aquired with the exclusion of previously detected point sources. Similarly, the spectra of the backgrounds for specific regions were obtained. In some cases, blank sky event lists (see Carter & Read 2007) were used for creating background spectrum corresponding to a proper region. For each spectrum response matrices and effective area files were produced. For the latter, detector maps needed for extended emission analysis were also created. Finally, the spectra were then fitted using XSPEC 11.

[3]http://xmm.esac.esa.int/external/xmm_science/gallery/utils/images.shtml

Table 2.3: Parameters of X-ray observations of studied galaxies

NGC	Obs. ID	Obs. date	Exp. time[a]	pn filter	pn obs. mode[b]	MOS filter	MOS obs. mode[b]	nH[c]
4254	0147610101	2003-06-29	43.2 (12.8)	Thin	EF	Thin	FF	2.81
4302*	0306060101	2005-12-05/06	96.5 (76.5)	Medium	FF	Medium	FF	2.53
4321	0106860201	2001-12-28/29	36.6 (3.1)	Medium	EF	Medium	FF	1.97
4388	0110930701	2002-12-12	11.9 (6.9)	Thin	EF	Medium	FF	2.58
4438	0210270101	2004-12-19	26.8 (24.6)	Thin	FF	Thin	FF	2.31
4501	0112550801	2001-12-04	14 (2.9)	Medium	EF	Thin	FF	2.62
4569	0200650101	2004-12-13/14	66 (49)	Thin	EF	Medium	FF	2.82

* Together with NGC 4298.
[a] Total time in ksec with clean time for pn camera in brackets.
[b] Observing mode: FF - Full Frame, EF - Extended Full Frame.
[c] Column density in [10^{20} cm^{-2}] weighted average value after LAB Survey of Galactic H I, see Kalberla et al. (2005).

Chapter 3

Results

3.1 NGC 4254

NGC 4254 is an Sc galaxy situated outside the cluster X-ray cloud (Böhringer et al. 1994), at the distance of $3\overset{\circ}{.}56$ from the centre (1.07 Mpc in the sky plane). It is a normal star-forming galaxy with no signs of any gas deficiency. A thorough presentation and analysis of its radio data can be found in Soida et al. (1996), as well as in Chyży (2008).

The extended X-ray emission roughly resembles the disturbances of Hα emission and star formation (Fig. 3.1 and Chyży et al. 2007), with no enhancements present in the outer parts of the disk, especially southern, where a polarized ridge of the radio emission is visible (Soida et al. 1996 and Chyży 2008). A bright peak visible in the southeastern part of the disk is due to a strong point source, possibly an ultra luminous X-ray source. Such sources are often associated with colliding systems, as galactic interactions produce higher star formation rate, which may result in forming of more massive young X-ray binaries (see Soria & Wong 2006). This would be in agreement with the observations of NGC 4254, suspected of tidal interactions with a dark galaxy VIRGO HI 21 (Minchin et al. 2007, Chyży 2008).

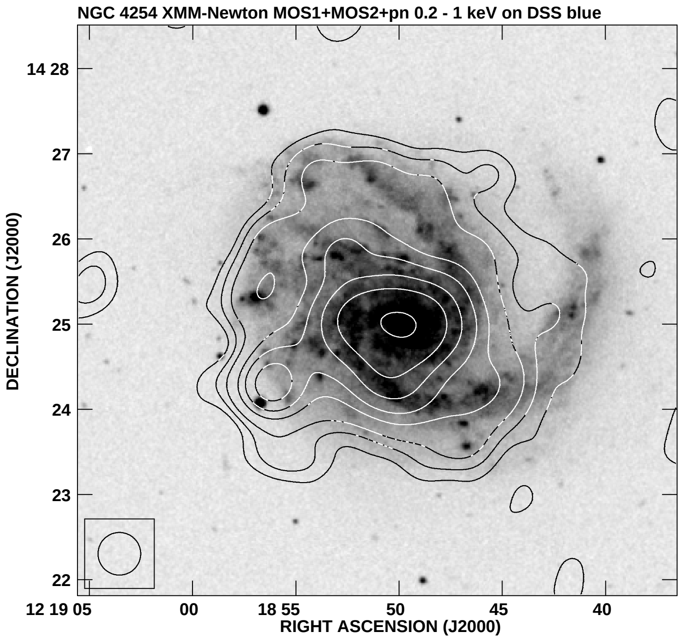

Figure 3.1: The map of soft X-ray emission from NGC 4254 in the 0.2 - 1 keV band overlaid onto the DSS blue image. The contours are 3, 5, 8, 16, 25, 40, 60, 100 × rms. The map is convolved to the resolution of 30″. The beam size is shown in the bottom left corner of the figure.

3.2 NGC 4298 and NGC 4302

NGC 4298 and NGC 4302 are two Sc galaxies (NGC 4302 seen edge-on) located at the distance of about 3°.1 (930 kpc in the sky plane) from Virgo A. These galaxies probably interacts tidally (e.g. Koopmann & Kenney 2004).

The most distinct feature in the map of the total power intensity (Fig. 3.2) is an eastern extension. At the same position a faint galaxy PGC 169114 is visible, however it seems not to be a source of a measureable radio emission, as checked with the NVSS (Condon et al. 1998) and FIRST (Becker et al. 2003) data. The apparent polarization B-vectors are plane-parallel, however they are inclined towards the eastern extension.

An extension visible south of NGC 4298 is due to a background NVSS radio source J122131+143352 with a total flux density (at 1.4 GHz) of 12.7 mJy (Condon 1998).

The peak of polarized intensity visible in NGC 4302 (Fig. 3.3) is shifted and elongated towards NGC 4298. This may support the idea of possible interactions. Also bulk of extended polarized intensity can be found in the

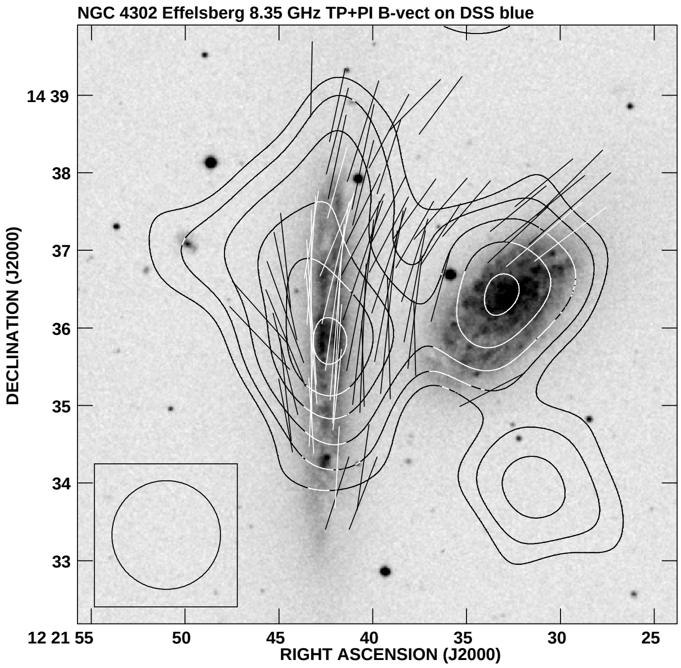

Figure 3.2: The total power map of NGC 4298 and NGC 4302 at 8.35 GHz with apparent B-vectors of polarized intensity overlaid onto the DSS blue image. The contours are 3, 5, 8, 12, 16, 20 × 0.3 mJy/b.a.. A vector of 1′ length corresponds to the polarized intensity of 0.25 mJy/b.a. The map resolution is 1.′5. The beam size is shown in the bottom left corner of the figure.

region between galaxies, which suggest ordered intergalactic magnetic field. Although NGC 4298 is of the same Sc-type as NGC 4302 it lacks a measurable polarized emission. This is most likely caused by the depolarization within the beam, as the galaxy is nearly face-on and the beamsize is roughly of the same size as the galaxy. A small patch of the polarized emission visible north of NGC 4298 and apparent polarization B-vectors aligned with the direction to NGC 4302 provide more arguments for interactions between both galaxies.

In the rotation measure map of NGC 4302 (Fig. 3.4) a negative peak of -135 rad/m^2 can be easily seen at the end of the eastern total power extension. Regions of positive RM, with values of +110 rad/m^2 are placed in the nortern part of the galaxy and at the position of the companion galaxy NGC 4298. An area of quite high negative RM around -60 rad/m^2 lies outside the optical image of NGC 4298 northwards where a small peak of polarized intensity and higher polarization degree can be found.

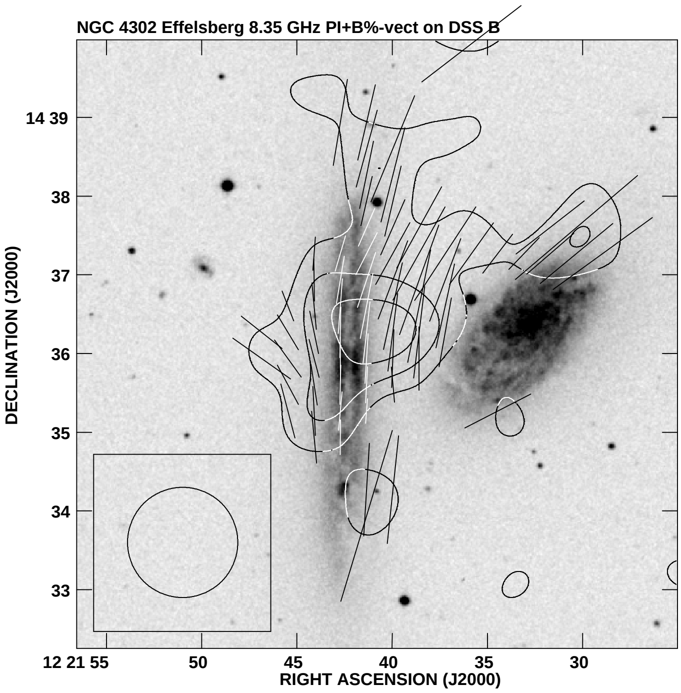

Figure 3.3: The map of polarized intensity of NGC 4298 and NGC 4302 at 8.35 GHz with apparent B-vectors of polarization degree overlaid onto the DSS blue image. The contours are 3, 5, 7 $\times$ 0.07 mJy/b.a.. A vector of $1'$ length corresponds to the polarization degree of 15%. The map resolution is $1\overset{'}{.}5$. The beam size is shown in the bottom left corner of the figure.

Weak X-ray emission visible in the region between galaxies (Fig. 3.5), as well as in an extension to the east from the disk of NGC 4302 provide more clues for a tidal encounter. Even the existence of a bright X-ray source, possibly an ULX, in the eastern side of the disk of NGC 4298 may suggest tidal interactions. In contrast to the radio extension, the X-ray appandage to the northeast from the centre of NGC 4302 is due to a background source. However, similar extension to the southeast aligned with the direction to the NGC 4298 very likely originates in the galactic halo. It is shifted from the disk in the same direction as the polarized intensity extension.

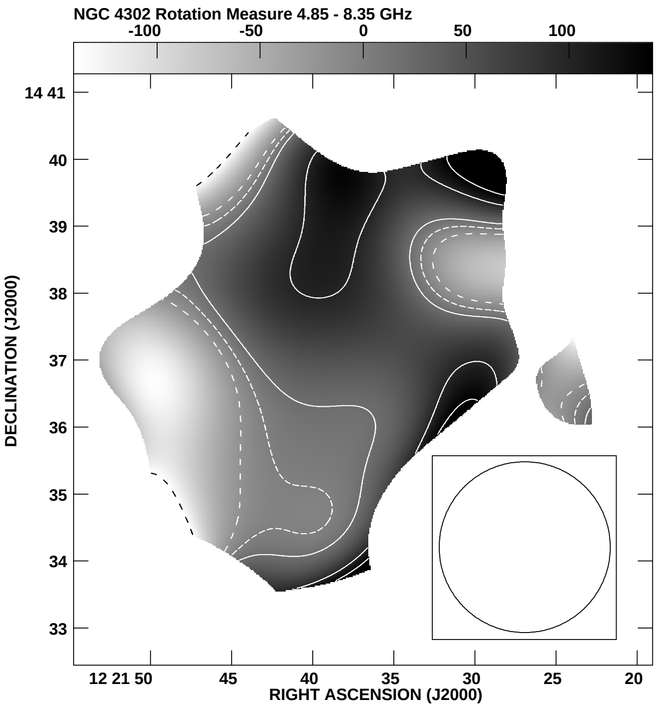

Figure 3.4: The map of the rotation measure between 4.85 and 8.35 GHz of NGC 4298 and NGC 4302. The contours are -7, -1, 0, 1, 5, 7 × 20 rad/m^2. The map resolution is 2.′5. The beam size is shown in the bottom right corner of the figure.

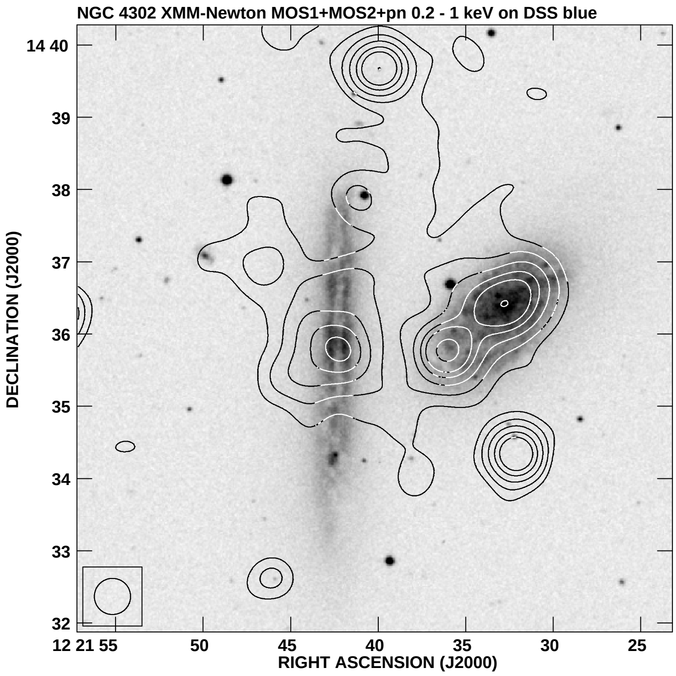

Figure 3.5: The map of soft X-ray emission from NGC 4298 and NGC 4302 in the 0.2 - 1 keV band overlaid onto the DSS blue image. The contours are 3, 5, 8, 12, 16, 25 $\times$ rms. The map is convolved to the resolution of $30''$. The beam size is shown in the bottom left corner of the figure.

3.3 NGC 4321

NGC 4321 is a grand-design barred spiral galaxy of SABb type. It is located at the distance of 3.°9 from the cluster core to the north (1.17 Mpc in the sky plane), what places it in the Virgo Cluster outskirts. This relatively unperturbed galaxy shows a faint H I tail extending to the southwest (Knapen 1993).

The total power emission (Fig. 3.6) is roughly symmetric being slightly more extended to the north. This is consistent with the observations of Urbanik et al. (1986) at 10.7 GHz. The disk contains three radio background sources. Two of them were found in the NVSS as J122258+155052, and J122251+154941 with the total fluxes at 1.49 GHz of 41.2 mJy, and 79.8 mJy, respectively. The third source, cataloged by the NVSS as J122258+154828 with the total flux of 55.7 mJy at 1.49 GHz, is in fact the supernova 1979C (Weiler et al. 1982), clearly visible in maps by Urbanik et al. (1986). At present it seems to be much weaker, with the flux density of only about 6 mJy at 1.49 GHz (Soida priv. comm.). The total power peak coincides with the optical centre of the galaxy.

The apparent polarization B-vectors follow well the optical spiral structure, especially in central parts of the galaxy, which host a distinct bar. The peak of polarized intensity is shifted northwards from the centre with the emission forming an S-shape structure in the central parts of the disk following the spiral structure (Fig. 3.7). The emission minima visible at both ends of the bar are due to a beam depolarization. The highest polarization degree (up to 30%) can be found in the northwestern part of the disk, where an H I ridge has been reported (Cayatte et al. 1990).

In the RM map of NGC 4321 two holes visible at the position of bar ends are due to depolarization. Southern part of the galaxy, where the polarized intensity and polarization degree is lower, is dominated by RMs of +50 – +110 rad/m^2 while in the north there is a large area of negative RM of -30 – -70 rad/m^2 with only small patch of positive RM of a few tens rad/m^2 in the northeast.

The X-ray morphology of the NGC 4321 is fairly symmetric (Fig. 3.9) with most of the emission coming from the central parts of the galaxy. Slight extensions to the southeast may be associated with an H I tail.

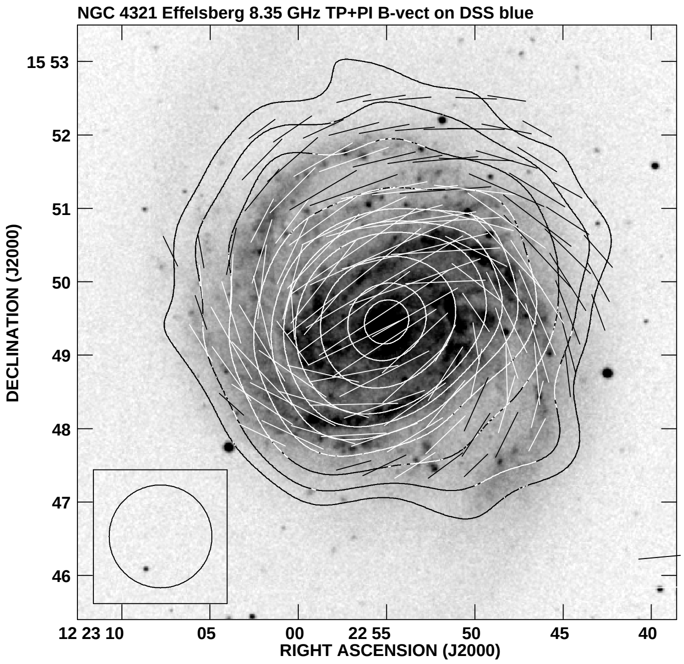

Figure 3.6: The total power map of NGC 4321 at 8.35 GHz with apparent B-vectors of polarized intensity overlaid onto the DSS blue image. The contours are 3, 5, 8, 12, 16, 20, 25, 40, 60, 70 × 0.3 mJy/b.a.. A vector of 1′ length corresponds to the polarized intensity of 0.5 mJy/b.a. The map resolution is 1.′5. The beam size is shown in the bottom left corner of the figure.

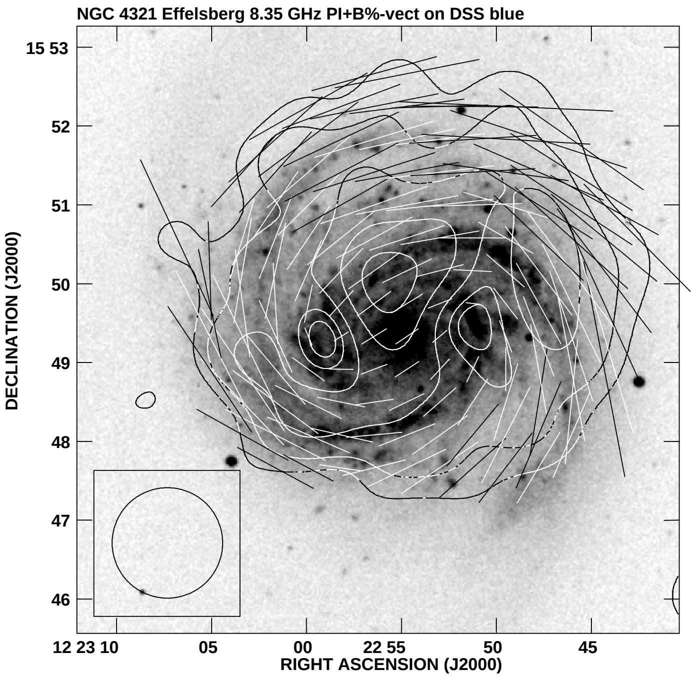

Figure 3.7: The map of polarized intensity of NGC 4321 at 8.35 GHz with apparent B-vectors of polarization degree overlaid onto the DSS blue image. The contours are 3, 5, 8, 12, 16 $\times$ 0.07 mJy/b.a.. A vector of $1'$ length corresponds to the polarization degree of 10%. The map resolution is $1\overset{'}{.}5$. The beam size is shown in the bottom left corner of the figure.

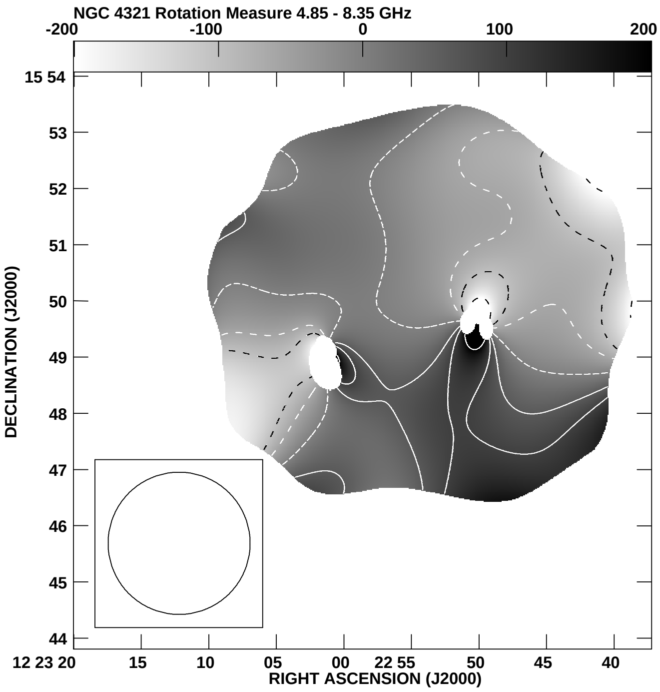

Figure 3.8: The map of the rotation measure between 4.85 and 8.35 GHz of NGC 4321. The contours are -10, -5, -3, 0, 3, 5, 10 × 20 rad/m^2. The map resolution is 2.′5. The beam size is shown in the bottom left corner of the figure.

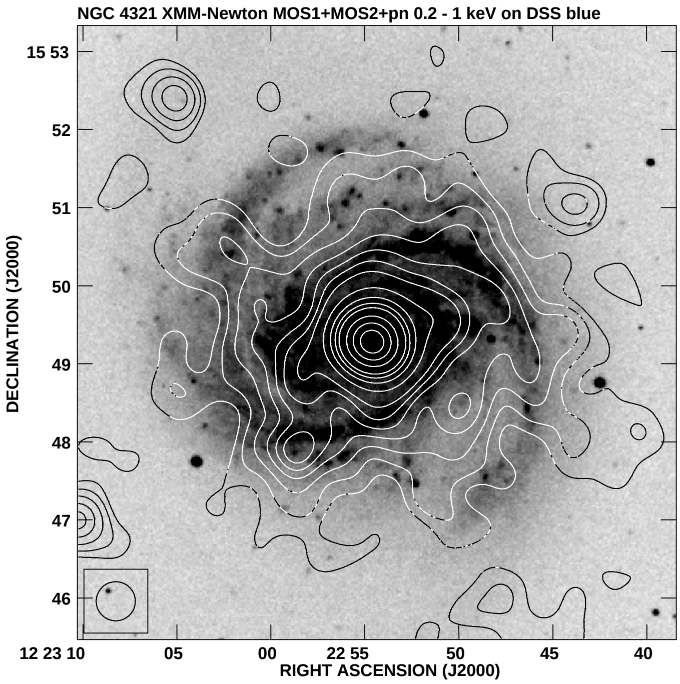

Figure 3.9: The map of soft X-ray emission from NGC 4321 in the 0.2 - 1 keV band overlaid onto the DSS blue image. The contours are 3, 5, 8, 12, 16, 20, 25, 40, 60, 80, 100, 150, 200, 250 × rms. The map is convolved to the resolution of 30″. The beam size is shown in the bottom left corner of the figure.

3.4 NGC 4388

NGC 4388 is a Seyfert 2 Sb-type spiral galaxy located close to the cluster core at the distance of only 1°.3 (390 kpc in the sky plane) from Virgo A. Observations of Cayatte et al. (1990 and 1994), as well as of Yoshida et al. (2004) suggest that this galaxy is heavily stripped and highly deficient in H I.

The total power emission (Fig. 3.10) is dominated by the central region of the galaxy (over 119 mJy at 1.4 GHz) and by two NVSS radio background sources placed symetrically on both sides of the galaxy centre (J122551+123951 and J122540+123958 with total flux densities of 4 mJy and 7.9 mJy, respectively). The low surface brightness extension to the west is very likely a mixture of NVSS radio background source J122528+124111 with a total flux density of 2.5 mJy at 1.4 GHz and FIRST radio background source J122519.2+123854 with a total flux density of 13.05 mJy at 1.4 GHz. However, the northern part of this extension (around R.A.$_{2000} = 12^{h}25^{m}27^{s}$, Dec.$_{2000} = 12°41'30''$) is not corresponding with any radio background source. It remains unclear whether it might be a real emission associated with the galaxy.

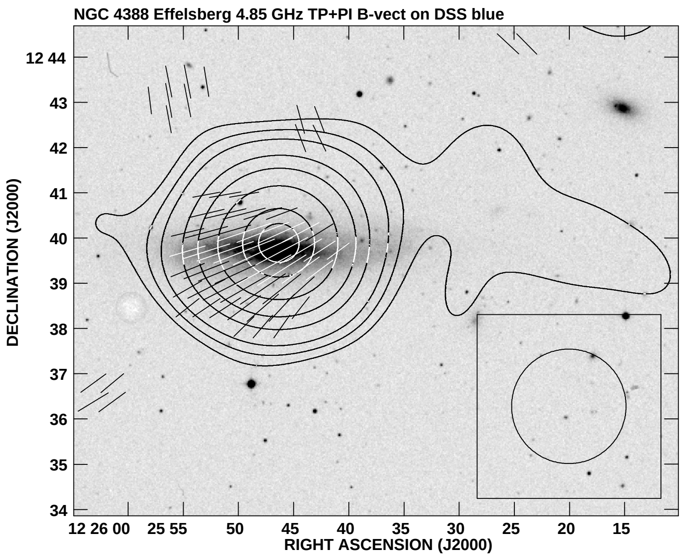

Figure 3.10: The total power map of NGC 4388 at 4.85 GHz with apparent B-vectors of polarized intensity overlaid onto the DSS blue image. The contours are 3, 5, 8, 16, 25, 40, 60, 70 × 0.9 mJy/b.a.. A vector of 1′ length corresponds to the polarized intensity of 0.5 mJy/b.a. The map resolution is 2.′5. The beam size is shown in the bottom right corner of the figure.

The apparent polarization B-vectors deviate significantly from the disk plane by about 30 degrees and are roughly aligned with the direction towards the cluster core (M 87), forming a "polarized fan" (Vollmer et al. 2007). Our low-resolution observations, though providing less details in the galactic disk than those of Vollmer et al. (2007), allow to detect low surface-brightness structures with better sensitivity. Such diffuse faint structures are important in the case of observations of a significantly stripped galactic disk. Our studies clearly shows that the magnetic field ordering occurs globally.

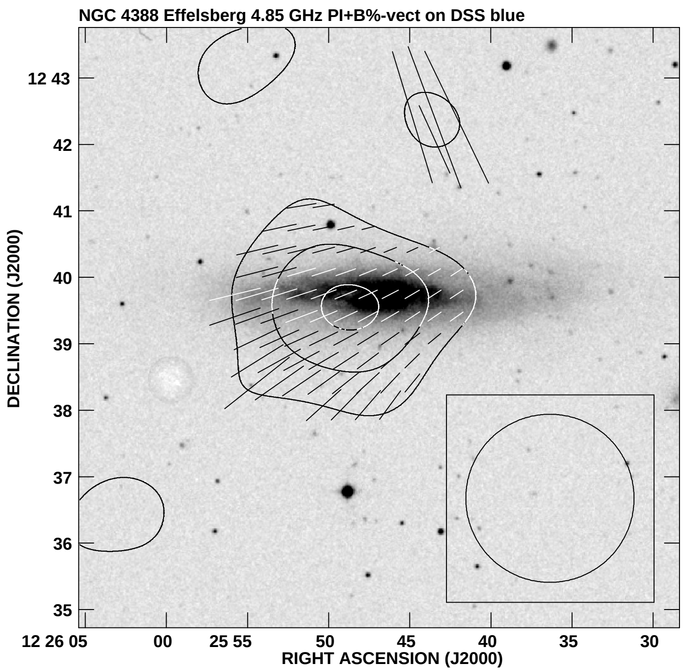

Figure 3.11: The map of polarized intensity of NGC 4388 at 4.85 GHz with apparent B-vectors of polarization degree overlaid onto the DSS blue image. The contours are 3, 5, 7 $\times$ 0.1 mJy/b.a.. A vector of $1'$ length corresponds to the polarization degree of 3.75%. The map resolution is $2\farcm5$. The beam size is shown in the bottom right corner of the figure.

In the X-ray map of NGC 4388 (Fig. 3.12) an extension to the northeast is visible just in the position of an Hα outflow reported by Yoshida et al. (2004). The asymmetry of the emission in the central parts of the disk is aligned in the same direction.

Low resolution sensitive wide field map of NGC 4388 (Fig. 3.13) suggests that the X-ray extension to the northeast might reach significant distances from the galaxy. More sensitive X-ray observations of NGC 4388 are desirable. They would allow to perform spectral analysis of the hot gas in this

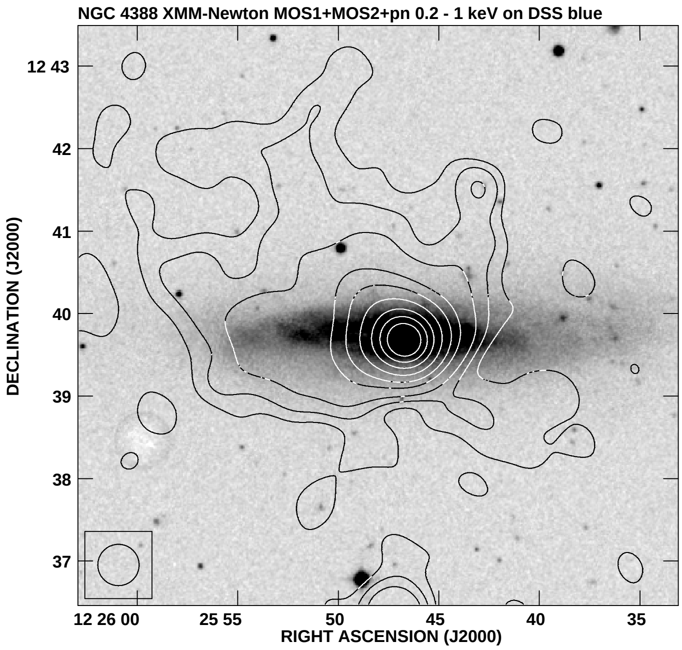

Figure 3.12: The map of soft X-ray emission from NGC 4388 in the 0.2 - 1 keV band overlaid onto the DSS blue image. The contours are 3, 5, 8, 16, 25, 40, 60, 80, 100 $\times$ rms. The map is convolved to the resolution of $30''$. The beam size is shown in the bottom left corner of the figure.

extension, which might help to answer the question whether the evolution of NGC 4388 is associated with tidal encounter between M 86 and NGC 4438 (Kenney et al. 2008), as the observed extension from NGC 4388 seems to reach as far as the vast X-ray halo of M 86 (see Sect. 3.5 and Fig. 3.17).

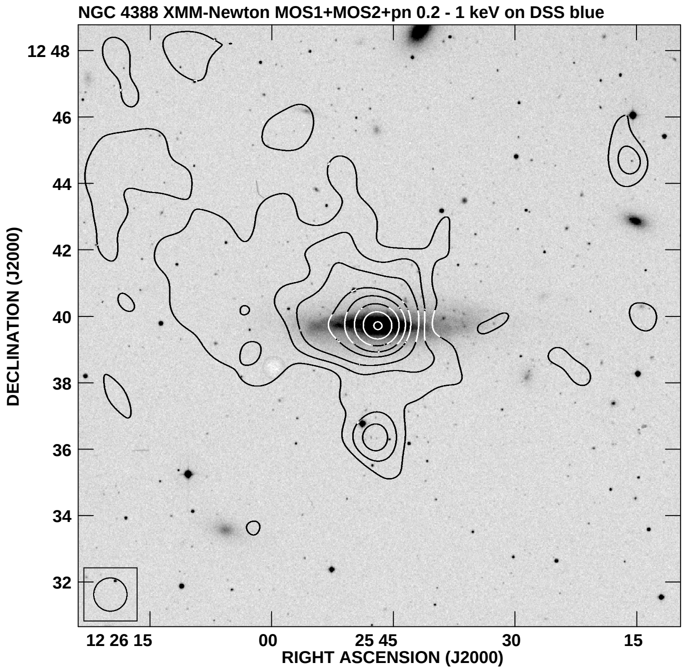

Figure 3.13: The wide field map of soft X-ray emission from NGC 4388 in the 0.2 - 1 keV band overlaid onto the DSS blue image. The contours are 3, 5, 8, 16, 25, 40, 60, 80 × rms. The map is convolved to the resolution of 1′. The beam size is shown in the bottom left corner of the figure.

3.5 NGC 4438

NGC 4438 is located close to the cluster centre, about 0.°9 from M 87 (270 kpc in the sky plane). Recent observations of Kenney et al. (2008) show that the galaxy most likely experienced a high-velocity collision with M 86, which resulted in its highly disturbed morphology, as well as in a high H I deficiency of NGC 4438. What is interesting, a companion galaxy NGC 4435 seems to be not related to the distortions of NGC 4438, in contrast to what was widely believed.

The peak of total power is at the position of the galactic centre (Fig. 3.14) with the apparent polarization B-vectors oriented parallel to the disk. However, the peak of the polarized intensity is shifted outwards from the disk (Fig. 3.15). It is displaced from the optical centre towards the southwest by about 55 arcseconds (4.6 kpc). At this position optical images show a complex of dust lanes that indicate strong compression effects. Other ISM tracers (H I, Hα, CO, FIR) also show emission to the west of NGC 4438 (e.g. Kenney et al. 1995, Chemin et al. 2005). High resolution Chandra X-ray observations of Machacek et al. (2004) also show bulks of hot gas west from the galaxy centre within the inner 30″. We find that most of polarized emission ($\simeq 74\%$) comes from the western side of the galaxy, which is also the direction towards M 86.

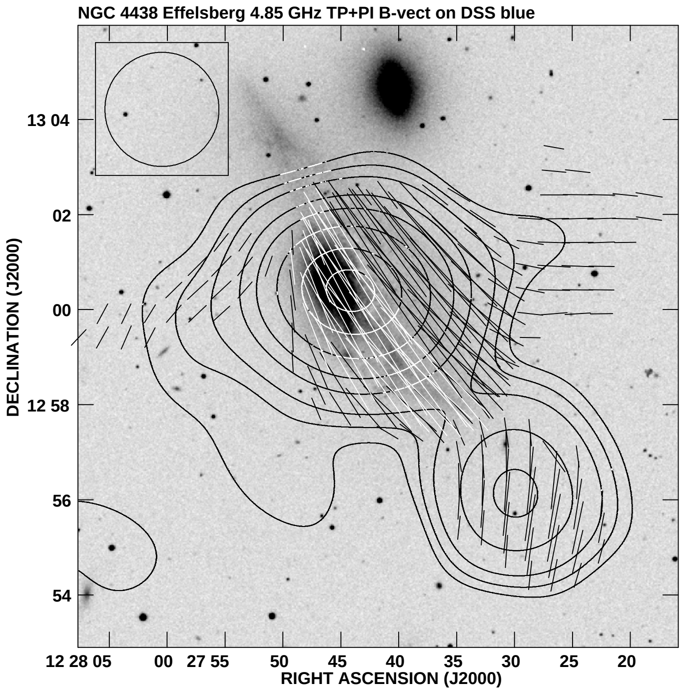

Figure 3.14: The total power map of NGC 4438 at 4.85 GHz with apparent B-vectors of polarized intensity overlaid onto the DSS blue image. The contours are 3, 5, 8, 16, 25, 40, 60, 75 × 0.7 mJy/b.a.. A vector of 1′ length corresponds to the polarized intensity of 0.5 mJy/b.a. The map resolution is 2.′5. The companion galaxy NGC 4435 is visible in the north. The beam size is shown in the top left corner of the figure.

The tail extending towards the southwest visible on both total power and polarized intensity maps (Figs. 3.14 and 3.15) is caused by two unresolved background sources, blended with a large beam and well visible in the map by Condon (1987) at 1.49 GHz. These are the NVSS radio sources J122730.6+125629 and J122728.5+125535 with total flux densities (at 1.4 GHz) of 38.52 mJy and 19.76 mJy (Condon 1998), respectively. Another weak radio source is responsible for the total power extension to the south. It is J122747.6+125647 with total flux of 2.48 mJy at 1.4 GHz.

In NGC 4438 both the total power (weakly) and the polarized intensity show also evidence for low surface brightness extraplanar features on both sides of the galactic disk: $\mathrm{RA}_{2000} = 12^{\mathrm{h}}27^{\mathrm{m}}48\overset{\mathrm{s}}{.}5$, $\mathrm{Dec}_{2000} = 13°00'59''$, and $\mathrm{RA}_{2000} = 12^{\mathrm{h}}27^{\mathrm{m}}26^{\mathrm{s}}$, $\mathrm{Dec}_{2000} = 13°01'30''$. The apparent polarization B-vectors are highly inclined to the disk (Fig. 3.15) and extend to at least 15 kpc ($3'$) from the optical centre of the galaxy. No emission is visible in these regions in neither maps of Condon (1987) nor NVSS (Condon et al. 1998).

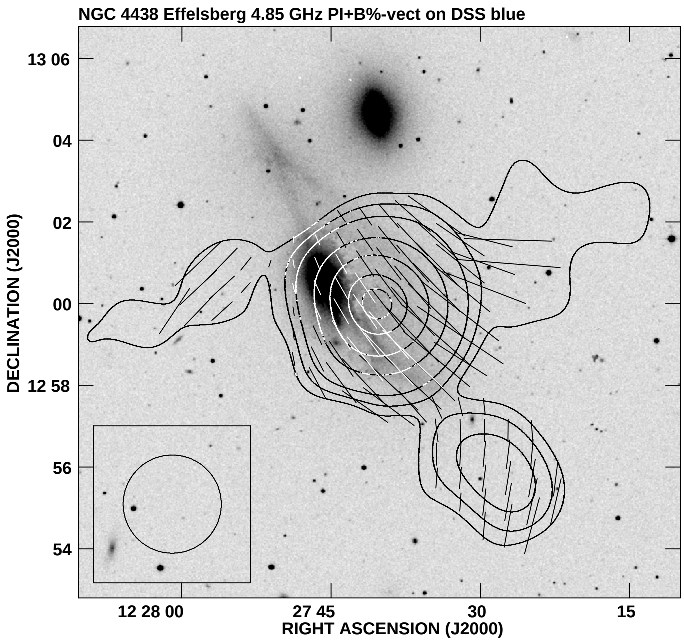

Figure 3.15: The map of polarized intensity of NGC 4438 at 4.85 GHz with apparent B-vectors of polarization degree overlaid onto the DSS blue image. The contours are 3, 5, 8, 16, 25, 35, 40 × 0.07 mJy/b.a.. A vector of $1'$ length corresponds to the polarization degree of 6%. The map resolution is $2\overset{'}{.}5$. The beam size is shown in the bottom left corner of the figure.

On the other hand, discussed extensions seem to be accompanied by the hot gas emision visible in the X-ray map of NGC 4438 (Fig. 3.16). A strong gradient in the northern part of the disk is due to the limit of the field of view of the pn camera. The map shows also a hot gas tail-like halo extending southwestwards. A wide field map (Fig. 3.17) reveals a giant X-ray cloud linking NGC 4438 to M 86. This could also be another evidence of the past collision. A strong gradient visible in the western egde of the map is due to the limit of the field of view.

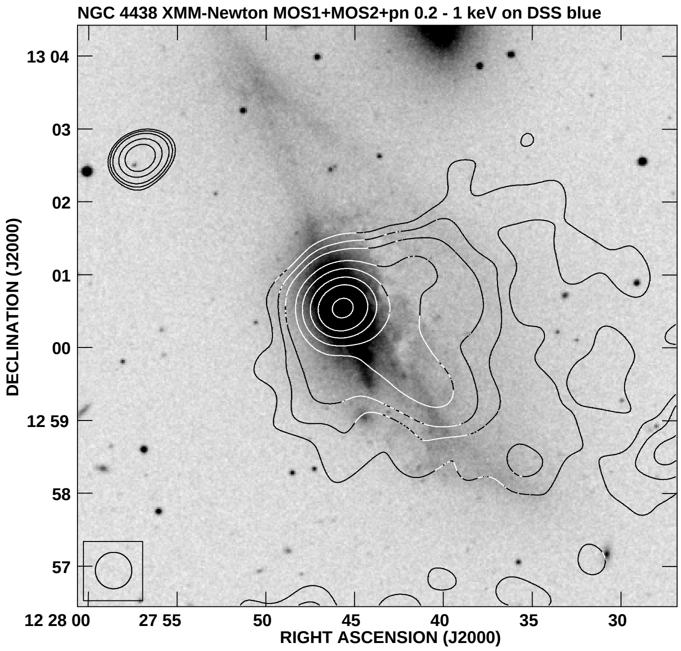

Figure 3.16: The map of soft X-ray emission from NGC 4438 in the 0.2 - 1 keV band overlaid onto the DSS blue image. The contours are 3, 5, 8, 16, 25, 40, 60, 100 × rms. The map is convolved to the resolution of 30″. The beam size is shown in the bottom left corner of the figure. A strong gradient in the northern part of the disk is due to the limit of the field of view of the pn camera.

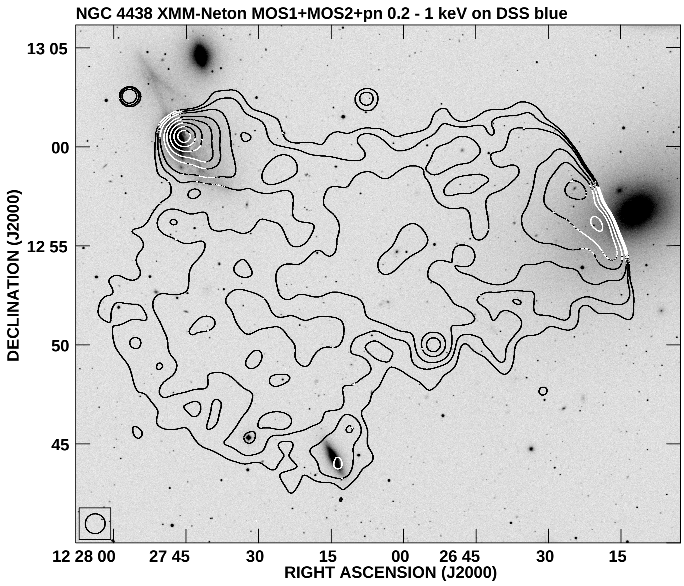

Figure 3.17: The map of soft X-ray emission from NGC 4438 and the halo of M 86 in the 0.2 - 1 keV band overlaid onto the DSS blue image. The contours are 3, 5, 8, 16, 25, 40, 60, 80 × rms. The map is convolved to the resolution of 1′. The beam size is shown in the bottom left corner of the figure. A strong gradient visible in the western egde of the map is due to the limit of the field of view.

3.6 NGC 4501

NGC 4501 is located at the distance of 2° from the cluster centre (600 kpc in the sky plane) to the north.

The total power emission at 10.45 GHz from this galaxy (Fig. 3.18) is symmetric and coincides with the optical disk. A slight extension outside the disk at $\mathrm{RA}_{2000} = 12^{\mathrm{h}}31^{\mathrm{m}}56^{\mathrm{s}}$, $\mathrm{Dec}_{2000} = 14°22'30''$ is produced by a weak background source visible in the NVSS map.

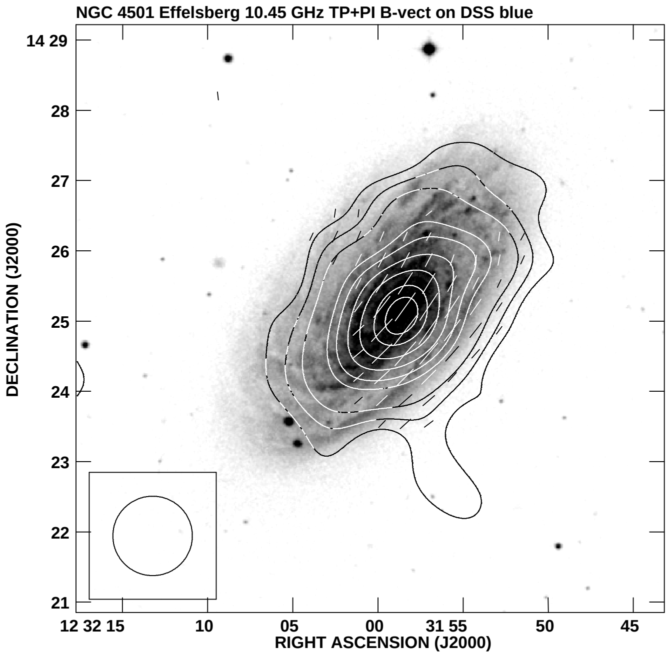

Figure 3.18: The total power map of NGC 4501 at 10.45 GHz with apparent B-vectors of polarized intensity overlaid onto the DSS blue image. The contours are 3, 5, 8, 16, 20, 25, 30, 35, 38 × 0.44 mJy/b.a.. A vector of 1′ length corresponds to the polarized intensity of 5 mJy/b.a. The map resolution is 1.′13. The beam size is shown in the bottom left corner of the figure.

The polarized emission is strongly shifted towards the southwest (Fig. 3.19). The asymmetry is significant, with 75% of the emission coming from the southwestern side of the disk. The degree of polarization reaches there about 20%.

In case of NGC 4501 the Faraday rotation measure changes gradually from +14 to +46 $\mathrm{rad/m^2}$ across the disk in the northwest-southeast direction. Its mean value is +30 $\mathrm{rad/m^2}$.

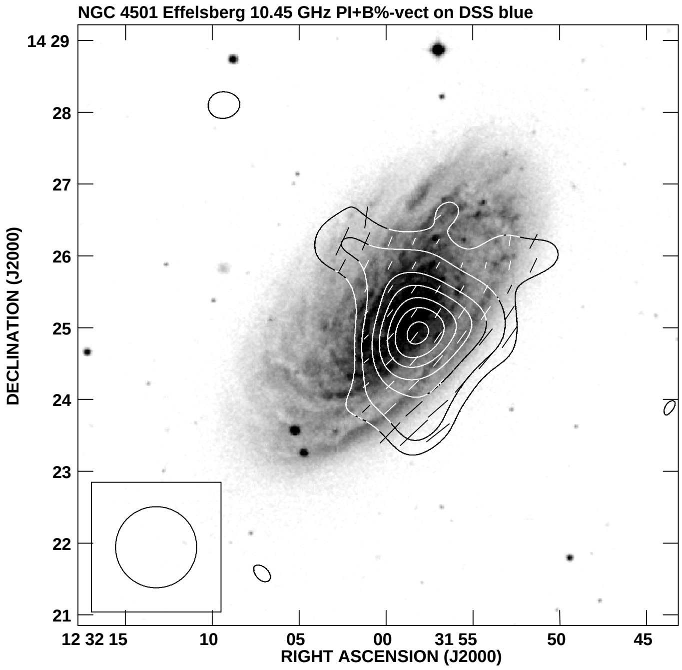

Figure 3.19: The map of polarized intensity of NGC 4501 at 10.45 GHz with apparent B-vectors of polarization degree overlaid onto the DSS blue image. The contours are 3, 5, 8, 10, 12, 13.5, 15 $\times$ 0.17 mJy/b.a.. A vector of 30″ length corresponds to the polarization degree of 50%. The map resolution is 1.′13. The beam size is shown in the bottom left corner of the figure.

The distribution of the hot gas in the disk of NGC 4501 (Fig. 3.21) resembles radio polarization data. However, X-ray data show faint extensions to the northeast, corresponding to the low density H I tail discovered by Vollmer et al. (2008). Hot gas extensions can provide further evidence of an intense ram-pressure stripping of this galaxy. The wide field map (Fig. 3.22) suggests the existence of a large envelope of hot gas around NGC 4501. Sensitive observations are desirable to verify the stripping scenario by determining temperature and origin of the gaseous tail, as well as of gas in the position of ridges of polarized intensity and H I. In the galaxy centre two maxima are visible, what most likely can be associated with nuclear activity of this galaxy.

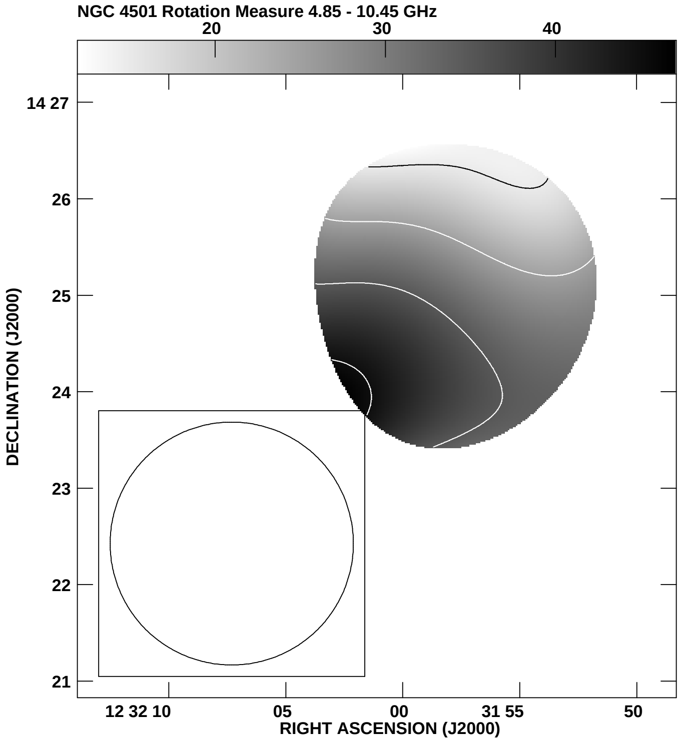

Figure 3.20: The map of the rotation measure between 4.85 and 10.45 GHz of NGC 4501. The contours are 3, 5, 7, 9 × 5 rad/m^2. The map resolution is 2$'$.5. The beam size is shown in the bottom left corner of the figure.

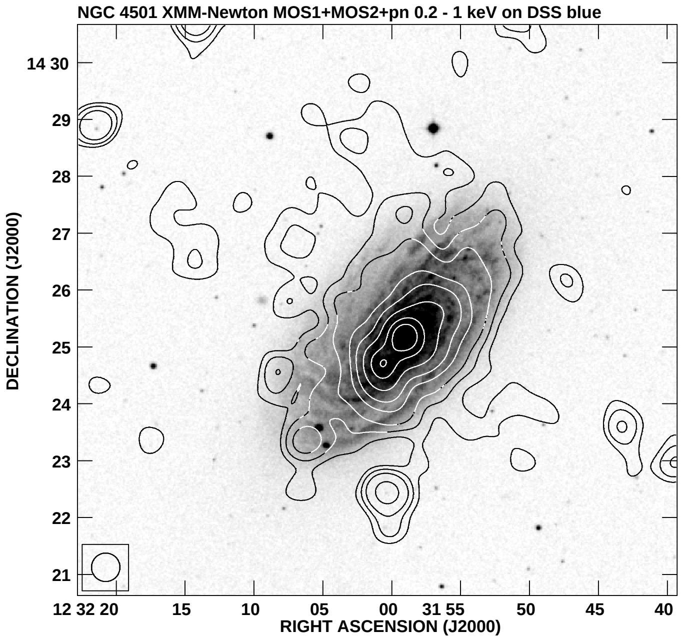

Figure 3.21: The map of soft X-ray emission from NGC 4501 in the 0.2 - 1 keV band overlaid onto the DSS blue image. The contours are 3, 5, 8, 16, 25, 40, 60, 75 × rms. The map is convolved to the resolution of 30″. The beam size is shown in the bottom left corner of the figure.

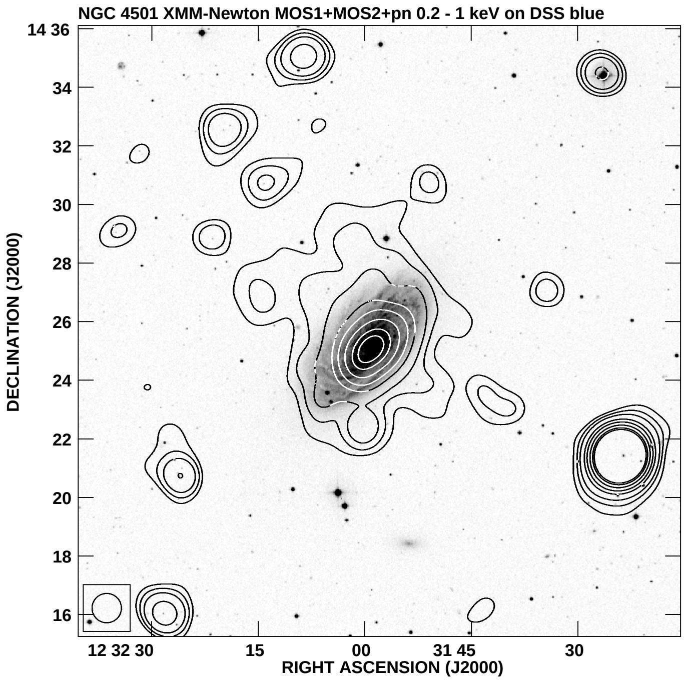

Figure 3.22: The wide field map of soft X-ray emission from NGC 4501 in the 0.2 - 1 keV band overlaid onto the DSS blue image. The contours are 3, 5, 8, 16, 25, 40, 60, 75 $\times$ rms. The map is convolved to the resolution of $1'$. The beam size is shown in the bottom left corner of the figure.

3.7 NGC 4535

NGC 4535 is a grand-design spiral galaxy located in the Southern Extension of the Virgo Cluster, formed around the giant elliptical M 49. The distance to the cluster core is of 4°.3 (1.29 Mpc in the sky plane).

Optical images show a very regular spiral structure of NGC 4535; it also has a quite symmetric H I distribution (Cayatte et al. 1990). This is reflected in a symmetric distribution of total intensity, with its peak roughly situated at the galaxy's centre (Fig. 3.23).

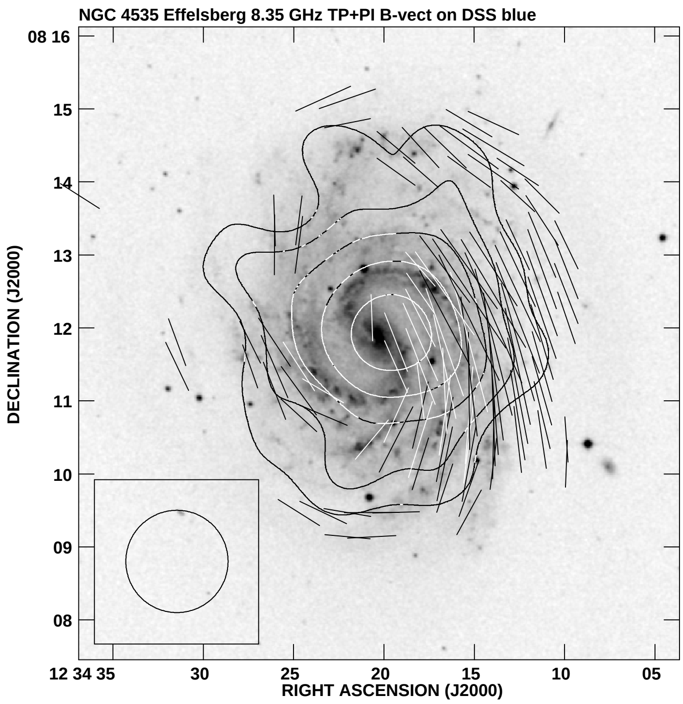

Figure 3.23: The total power map of NGC 4535 at 8.35 GHz with apparent B-vectors of polarized intensity overlaid onto the DSS blue image. The contours are 3, 5, 8, 12, 17 × 0.3 mJy/b.a.. A vector of 1′ length corresponds to the polarized intensity of 0.3 mJy/b.a. The map resolution is 1′.5. The beam size is shown in the bottom left corner of the figure.

The map of polarized intensity at 4.85 GHz reveals a strong asymmetry with 75% of the polarized flux coming from the western half of the disk (Fig. 3.24). It is confirmed by observations at 8.35 GHz (Fig. 3.25), where the asymmetry remains at a similar level (73%). Therefore, it cannot be caused by an effect of a large beam. The peak of the polarized emission is located in the western optical spiral arm, which may suggest strong compression effects. The extension to the northeast, visible in the low resolution map is due to a background source. The apparent polarization B-vectors follow generally the spiral structure. The degree of polarization varies across the disk from 15% in the eastern disk half to 30% in its western half, reaching 40% in the western outskirts of the optically visible galaxy.

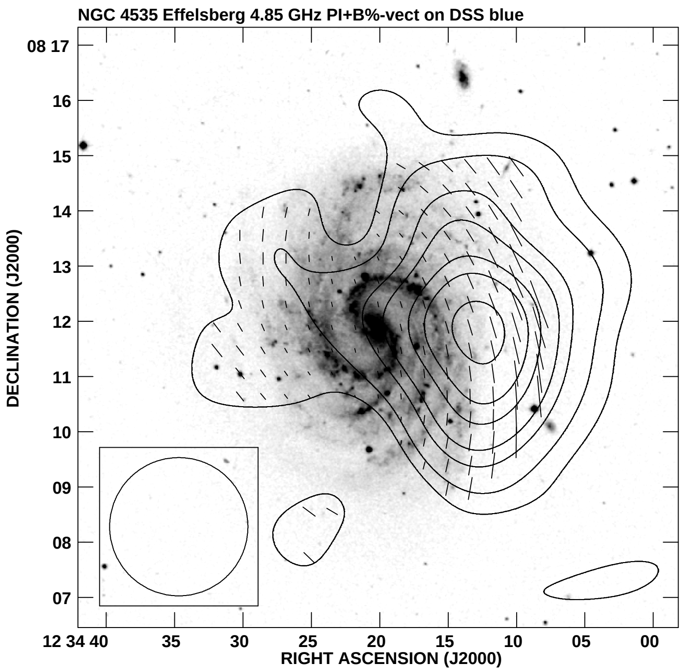

Figure 3.24: The map of polarized intensity of NGC 4535 at 4.85 GHz with apparent B-vectors of polarization degree overlaid onto the DSS blue image. The contours are 3, 5, 8, 10, 13, 15, 18 × 0.1 mJy/b.a.. A vector of 1′ length corresponds to the polarization degree of 60%. The map resolution is 2.′5. The beam size is shown in the bottom left corner of the figure.

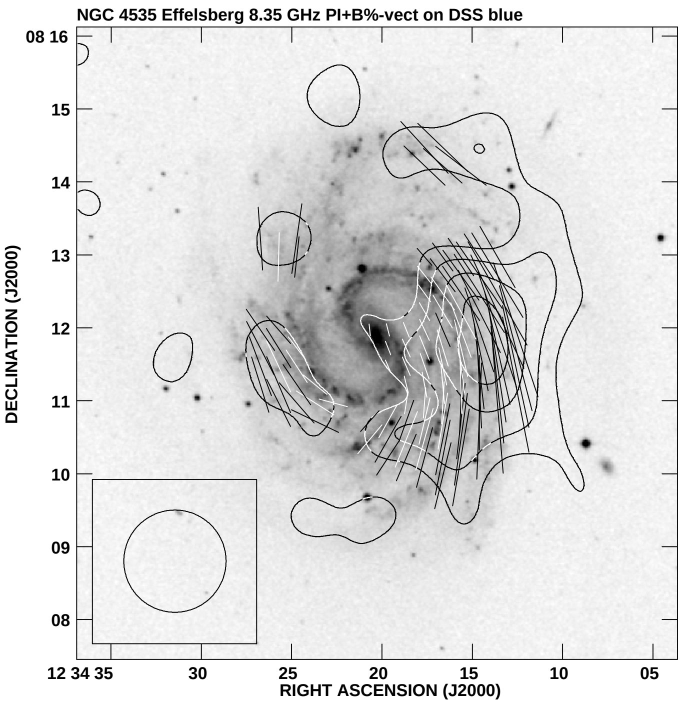

Figure 3.25: The map of polarized intensity of NGC 4535 at 8.35 GHz with apparent B-vectors of polarization degree overlaid onto the DSS blue image. The contours are 3, 5, 7, 9 × 0.07 mJy/b.a.. A vector of 1′ length corresponds to the polarization degree of 20%. The map resolution is 1.′5. The beam size is shown in the bottom left corner of the figure.

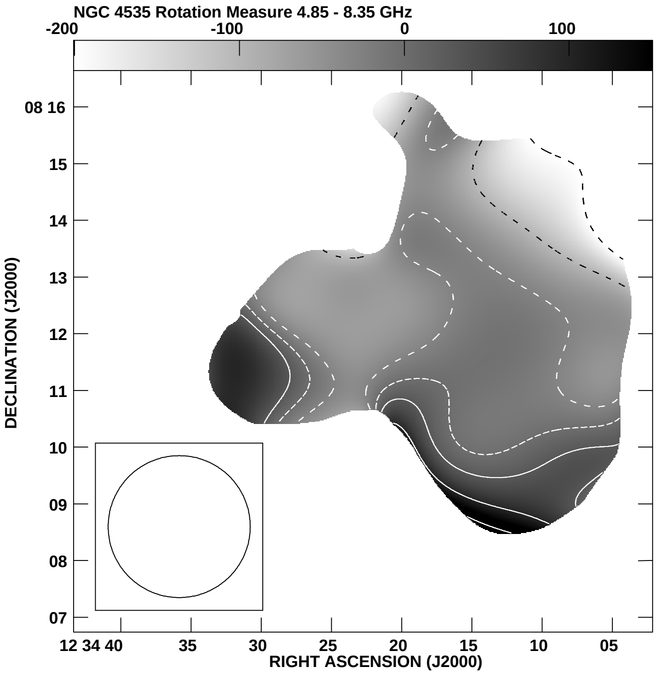

Figure 3.26: The map of the rotation measure between 4.85 and 8.35 GHz of NGC 4535. The contours are -20, -10, -3, 0, 3, 10, 20 × 10 rad/m^2. The map resolution is 2.′5. The beam size is shown in the bottom left corner of the figure.

3.8 NGC 4548

NGC 4548 is located in the northern part of the Virgo Cluster at the distance of 2.4° (720 kpc in the sky plane) from Virgo A. It is an anaemic SBb galaxy being extremely poor in neutral gas (Cayatte et al. 1990). It shows a generally weak total power emission (Fig. 3.27).

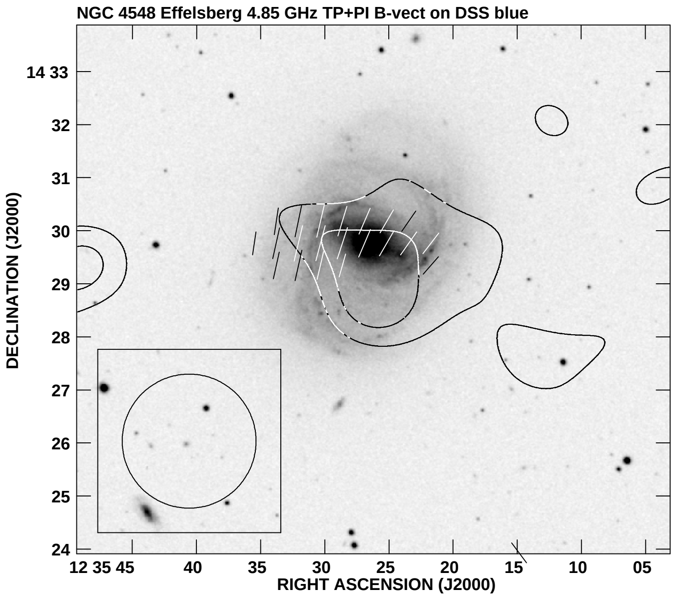

Figure 3.27: The total power map of NGC 4548 at 4.85 GHz with apparent B-vectors of polarized intensity overlaid onto the DSS blue image. The contours are 3, 4 × 0.77 mJy/b.a.. A vector of 1′ length corresponds to the polarized intensity of 0.84 mJy/b.a. The map resolution is 2.′5. The beam size is shown in the bottom left corner of the figure.

The polarized intensity is only slightly above the noise level (Fig. 3.28) and the degree of polarization reaches ≈ 15%, but this quite a high value may be caused by low radio emission which makes the measurements uncertain. Also the resolution of our observations is quite poor. However, at such low level of radio emission, 4.85 GHz is probably the highest frequency possible to study this galaxy. The polarized emission is concentrated in the central parts of the galaxy, along the bar. It coincides with an east-west elongated hole in the H I emission (Vollmer et al. 1999). The polarized emission peak is on the eastern end of the bar and the apparent polarization B-vectors are roughly perpendicular to the bar, which is quite surprising.

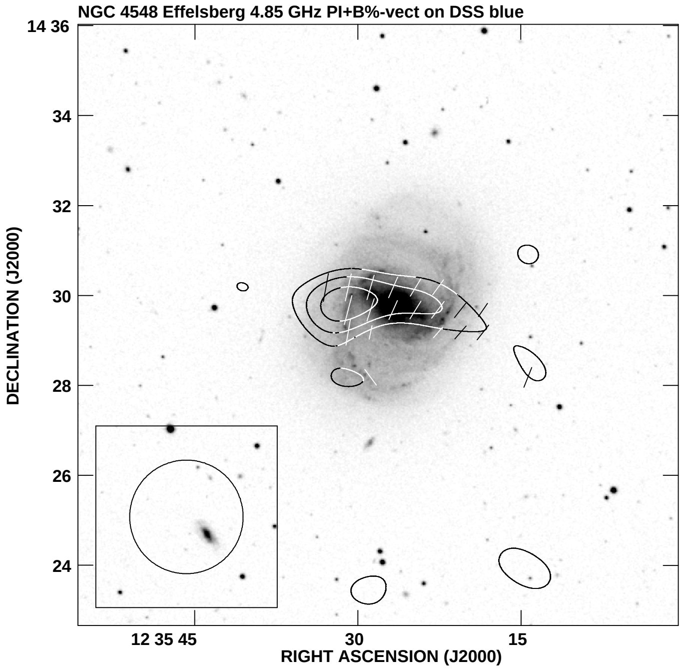

Figure 3.28: The map of polarized intensity of NGC 4548 at 4.85 GHz with apparent B-vectors of polarization degree overlaid onto the DSS blue image. The contours are 3.5, 4.5, 5.5 × 0.09 mJy/b.a.. A vector of 1′ length corresponds to the polarization degree of 30%. The map resolution is 2.′5. The beam size is shown in the bottom left corner of the figure.

3.9 NGC 4569

NGC 4569 is an SABa galaxy situated quite close to the cluster centre, at the distance of 1.°66 (500 kpc in the sky plane) from Virgo A. This is an anaemic galaxy showing extended radio lobes unusual for a normal spiral (Chyży et al. 2006). For a thorough presentation and disscusion of the radio data from this galaxy see Chyży et al. (2006).

The high resolution map of the X-ray emission (Fig. 3.29) from this galaxy shows hot gas extensions visible on both sides of the optical disk. They reach up to 5 kpc (1′) on the eastern and 8.5 kpc (1.′7) on the western side and coincide with the observed radio features. An emission peak in the northwestern disk outskirts is due to a background source. The map with a lower resolution, thus more sensitive to extended structures (Fig. 3.30) reveals a giant hot gas halo around the galaxy. North of the galaxy, still within the X-ray halo, lies an irregular galaxy, IC 3583, with which NGC 4569 is suspected to interact (Tschöke et al. 2001 and Chyży et al. 2006).

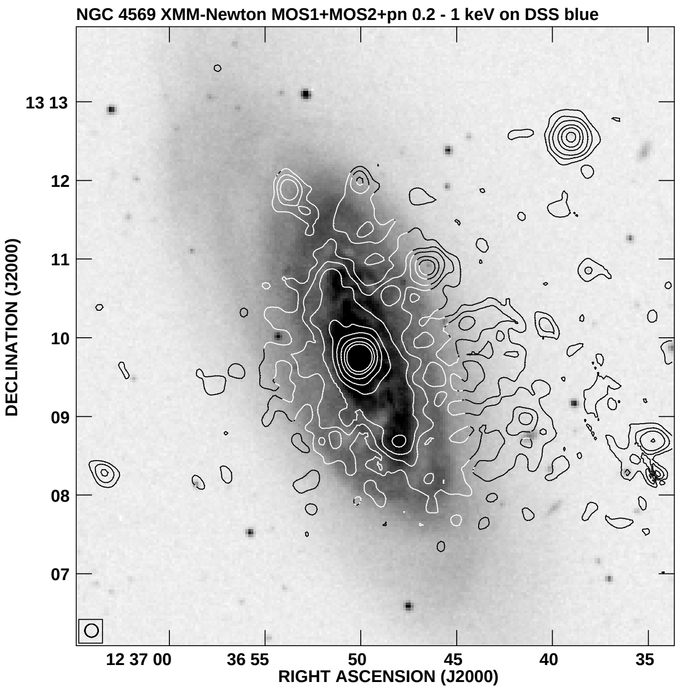

Figure 3.29: The map of soft X-ray emission from NGC 4569 in the 0.2 - 1 keV band overlaid onto the DSS blue image. The contours are 5, 8, 16, 25, 40, 60, 100 × rms. The map resolution is 10″. The beam size is shown in the bottom left corner of the figure.

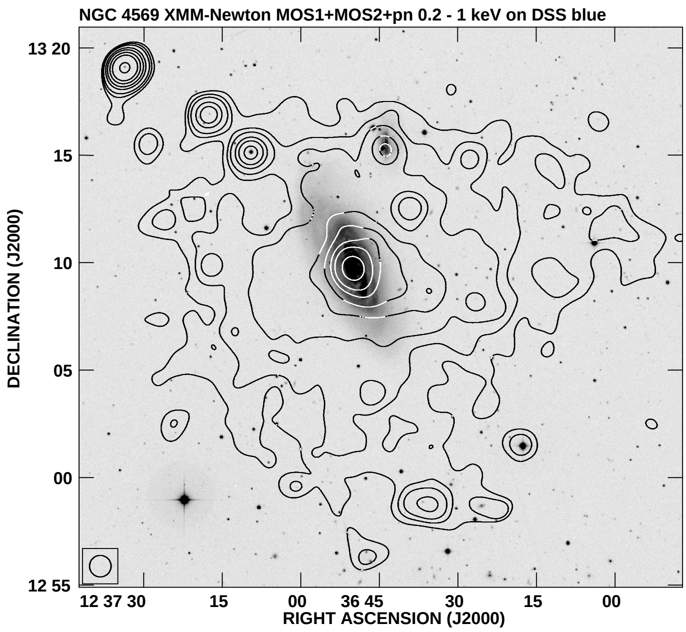

Figure 3.30: The map of soft X-ray halo around NGC 4569 in the 0.2 - 1 keV band overlaid onto the DSS blue image. The contours are 3, 5, 8, 16, 25, 40, 60, 120 × rms. The map is convolved to the resolution of 1′. The beam size is shown in the bottom left corner of the figure.

Table 3.1: Integrated data of studied galaxies

NGC	$S_{4.85\mathrm{GHz}}$ (TP) [mJy]	$S_{4.85\mathrm{GHz}}$ (POL) [mJy]	% p 4.85 GHz	$S_{8.35\mathrm{GHz}}$ (TP) [mJy]	$S_{8.35\mathrm{GHz}}$ (POL) [mJy]	% p 8.35 GHz
4298	30.2±2.5[a]	2.8±0.3[a]	9.3±1.3[a]	6.3±0.6	0.4±0.1	6.3±1.7
4302	30.2±2.5[a]	2.8±0.3[a]	9.3±1.3[a]	14.2±1	1.6±0.2	11.3±1.7
4321	95.7±5.3	6.3±0.5	6.6±0.6	68.3±3.6	5.7±0.4	8.3±0.7
4388	78.7±4.8	0.9±0.3	1.1±0.4	–	–	–
4438	86.8±6.5	5±0.6	5.8±0.8	–	–	–
4501	102.4±8.1	10.5±1	10.3±1.3	53.5±5.1*	6.8±1.6*	12.8±3.3*
4535	39.5±4.3	4.6±0.8	11.7±2.3	22±1.5	2.7±0.3	12.3±1.7
4548	5.7±1.8	0.6±0.3	11.2±6.2	–	–	–

% p – polarization degree.
TP = total power flux density, POL = polarized flux density.
[a] Due to a large beam at 4.85 GHz, NGC 4298 and NGC 4302 are unseparable. A value for both galaxies is presented.
[b] at 10.45 GHz.

Chapter 4

Discussion

In this chapter the magnetic properties of the studied galaxies are discussed, as well as their dependence on the nature of interactions exerted upon them by the cluster environment. In section 4.5, global characteristics of sample galaxies are presented and discussed, especially in terms of parameters related to star formation. The methods of derivation of thermal fractions, nonthermal indices, as well as of calculation of magnetic fields are briefly described. Values of calculated parameters for each galaxy are presented in tables 4.11 and 4.12.

4.1 Anaemic galaxies

A most obvious group of galaxies that are gas deficient and have less prominent star formation are anaemic galaxies. This class of objects in our sample is represented by two galaxies, NGC 4548 (Sect. 3.8) and NGC 4569 (Sect. 3.9). Both objects present high gas deficiency and mediocre star formation. However, this thesis shows that these objects present quite different characteristics. The first one, NGC 4548 (Figs. 3.27 and 3.28), is a highly gas deficient galaxy with a deficiency parameter of 0.8. The value of H I deficiency is presented throughout this thesis after Gavazzi et al. (2005) as a logarithmic difference between masses of neutral hydrogen in a field galaxy and a given galaxy. Gas deficiency parameters for all sample galaxies are presented in Table 4.11 at the end of Section 4.5. Parameter of 0.8 for NGC 4548 means that the galaxy is over 6 times less abundant in neutral hydrogen than a normal field galaxy of the same morphological type. This should be no surprising, as NGC 4548 is a very weak radio source. The integrated flux density (hence total luminosity) at 4.85 GHz is by a factor of 3 – 10 times lower than that of other spirals in the studied sample. It is worth noticing that another Virgo

Cluster object, NGC 4579, of similar morphological type and H I deficiency still has a total flux density a few times higher, even when the nuclear region of NGC 4579 is excluded (Becker et al. 1991, Nagar et al. 2005, Gallimore et al. 2006). Though NGC 4548 seems to be a "died-out" galaxy, it has significant total magnetic field of 6.3±1.8 μG, roughly 2 μG stronger than weakly forming stars late-type spirals observed by Chyży et al. (2007). The regular component of 2.1±0.9 μG is also stronger than in mentioned galaxies. Still, we should note that in the case of NGC 4548 calculated values for the total, and especially regular magnetic field are most likely their upper limits due to uncertainties of our measurements (see Sect. 3.8). Nevertheless, NGC 4548 shows lower thermal fraction not exceeding 20%, compared to 50-70% for galaxies from the work of Chyży et al.(2007). This could explain, at least partially, the difference in magnetic field strengths. NGC 4548 could simply have stronger overall nonthermal emission, which the radio – FIR correlation diagram seems to confirm (cf. Fig. 4.12 and Chyży et al. 2007 and Fig. 11 therein). As NGC 4548 is also gas deficient and forms stars at a very low rate (SFR $\simeq$ 0.26 - 0.30), higher nonthermal emission would mean stronger magnetic fields. This can be also associated with the past of NGC 4548. The galaxy is redder than a normal galaxy of its type in both $B - V$ and $U - B$ colours by $0\overset{\mathrm{m}}{.}14$ and $0\overset{\mathrm{m}}{.}35$ (Table 4.11), respectively, which suggests that the star forming activity may have significantly slowed down only recently. This would mean that the magnetic field is still partially preserved. Furthermore, interactions with the cluster environment, especially ram-pressure effects, could provide conditions to compressions and thus amplifications of the magnetic fields. As mentioned in Sect. 3.8, the magnetic field vectors seem to be perpendicular and not parallel to the bar. This also could be a sign of intense past interactions with the ICM, which led to significant gas deficiency of this galaxy.

The second anaemic galaxy in our sample, NGC 4569, shows completely different features. It is even more gas deficient than NGC 4548 (deficiency parameter of 1.07 (see Table 4.12), however shows impressive radio lobes, unusual for a normal spiral galaxy (Chyży et al. 2006). The diffuse western lobe has a spectral index of up to -1.4 while in the disk it does not exceed -1.0. On the other hand, in the eastern lobe a region of flat spectrum is present with a spectral index of -0.6. Chyży et al. (2006) argue that this can be explained by in-situ electron acceleration in a large-scale shock. NGC 4569 shows significant emission from the central parts of the disk with magnetic field vectors aligned with the major axis. Although an anaemic object, this galaxy shows unexpectedly strong total magnetic field of 8.7±2.7 μG. Our calculations were restricted to the disk only, therefore we cannot associate such a high value with radio lobes. This galaxy is however bluer in B-V colour by $0\overset{m}{.}11$ than a typical galaxy of the same type and at the same time redder in U-B colour by $0\overset{m}{.}17$ (Table 4.11). It could mean that we are observing this galaxy shortly after the end of the starburst phase what would explain significant strength of the magnetic field, though most likely it is now diminishing.

We performed a spectral analysis of our X-ray observations to search for clues about the origin and evolution of radio lobes. Extended soft X-ray emission from the galaxy (Fig. 3.29) was modelled by a simple fit of two temperature thermal plasma with a contribution from background point sources absorbed in the galactic foreground. The regions for which the spectra were aquired and fitted are presented in Fig. 4.1. The resulting parameters are shown in Table 4.1 and fluxes calculated using the model are shown in Table 4.2. Thermal plasma is represented here, as well as in other models in this thesis, by a mekal model, which is a model of an emission spectrum from hot diffuse gas based on the model calculations of Mewe and Kaastra (e.g. Mewe et al. 1985, Kaastra 1992). A contribution from background point sources is fitted with a simple power law, where photon index denotes the slope of the fit (e.g. Table 4.1). Our data could not be well fitted with a single temperature model, therefore, we used two temperature model, which allowed better parametrization. This model we could explain as an emission from a mixture of two thermal plasmas before reaching a thermal equilibrium. It seems to be a good approach in the case of studying outflows of the hot gas from the galactic disk. An additional emission well fitted with power law is included to take into account possible undetected background point sources. The spectral analysis of X-ray emission from hot gas chimneys coincident with unusual radio features, as well as Hα outflows, seems to support the scenario that giant radio lobes were produced through a galactic starburst phase and then compressed by the surrounding medium, as suggested by Chyży et al. (2006). This is because temperatures of outflowing gas are roughly the same as those for the disk (see Table 4.1), what suggests an effecient disk-to-halo energy trasport. Our data are not sensitive enough to perform spectral analysis of outer parts of the galactic halo. Their temperatures would directly answer the question, whether we are seeing shock heating in the surrounding medium. Nevertheless, the polarized "spur" visible in radio data coincides with a region of emission of the hottest gas (region 5), where the temperatures of both components are higher than for other regions. This could be a direct confirmation of an ongoing compression, though it may be a result of infalling gas, previously expelled from the galaxy, as simulations of Vollmer et al. (2004) suggest. The analysis of the nuclear region doesn't suggest that NGC 4569 is at present an active galaxy (as compared to NGC 4438 - see Sect. 4.3 and Table 4.3), what confirms that the radio lobes might be products of a past galactic starburst phase rather than of central activity.

Both galaxies, though anaemic, present significant differences in the observed features. We could explain such differences by proposing two different phases of past interactions with the cluster environment. Most likely significant gas deficiency was produced more rapidly in NGC 4569, as a result of a galactic starburst phase, which in turn could be triggered by past tidal encounter. In NGC 4548 gas deficiency could be just an effect of ram-pressure stripping of rather moderate intensity, which could turn the galaxy into a gas poor object, but with no clear signs of strong perturbations. Close distances of these galaxies to the cluster centre would support such scenarios which, require significant influence of the cluster environment. It is obvious that it will be strongest in the cluster core.

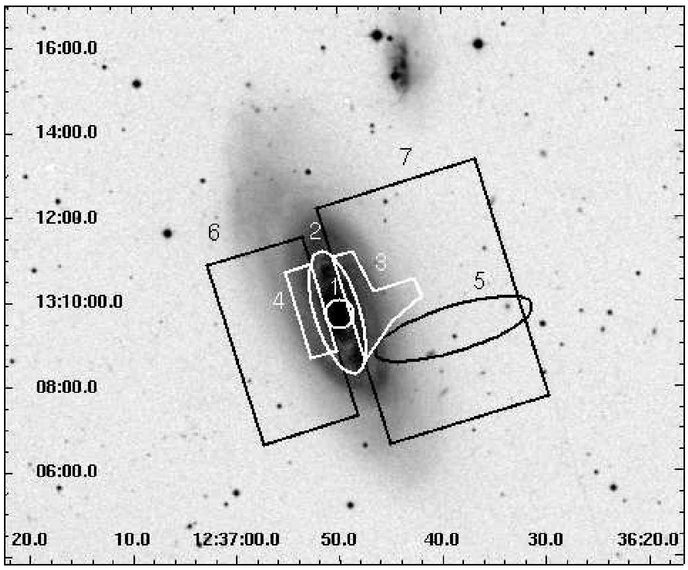

Figure 4.1: Regions of NGC 4569 for which the spectra were aquired. All background sources were extracted before creating the spectrum.

Table 4.1: Model fit parameters of selected regions in NGC 4569.

Reg. no.	kT_1 [keV]	kT_2 [keV]	Photon Index
1	0.21 ± 0.05	0.64 ± 0.03	$1.71^{+0.07}_{-0.09}$
2	$0.14^{+0.10}_{-0.04}$	0.46 ± 0.08	$1.26^{+0.25}_{-0.24}$
3	0.12 ± 0.01	0.47 ± 0.08	$1.11^{+0.17}_{-0.16}$
4	$0.15^{+0.06}_{-0.02}$	$0.61^{+0.07}_{-0.15}$	0.77 ± 0.24
5	$0.23^{+0.09}_{-0.08}$	$0.62^{+0.24}_{-0.17}$	$1.33^{+0.20}_{-0.21}$
6	0.12 ± 0.01	$0.48^{+0.07}_{-0.13}$	1.07 ± 0.11
7	0.10 ± 0.01	$0.47^{+0.06}_{-0.08}$	$1.16^{+0.12}_{-0.10}$

Table 4.2: 0.2 - 12 keV unabsorbed fluxes in $\mathrm{erg\,cm^{-2}s^{-1}}$ for modelled regions in NGC 4569.

Reg. no.	mekal 1	mekal 2	powerlaw	total
1	1.10e-14	5.75e-14	1.59e-13	2.27e-13
2	6.29e-15	1.63e-14	5.28e-14	7.54e-14
3	1.67e-14	1.52e-14	8.19e-14	1.14e-13
4	9.53e-15	1.04e-14	4.31e-14	6.31e-14
5	9.61e-15	9.28e-15	1.13e-13	1.32e-13
6	4.00e-14	2.23e-14	2.89e-13	3.57e-13
7	8.73e-14	5.56e-14	5.40e-13	6.88e-13

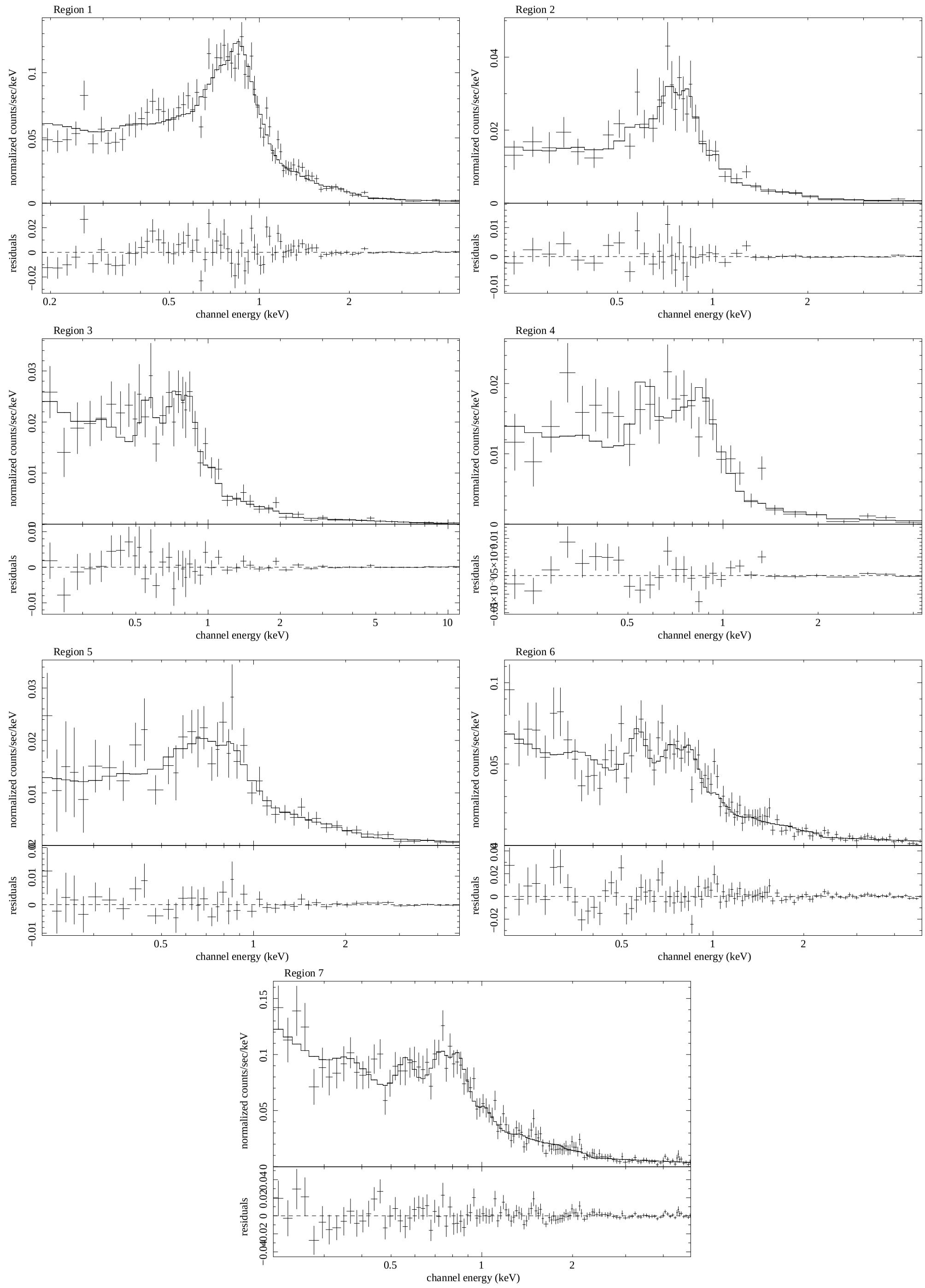

Figure 4.2: Model fits to the regions of NGC 4569. See tables 4.1 and 4.2.

4.2 Interactions with the ICM

High efficiency of the gas stripping, which may lead to significant gas deficiences in spiral galaxies, seems to be quite common in a cluster environment. Quantitative description is still being a subject of studies (e.g. Vollmer et al. 2001, Otmianowska-Mazur & Vollmer 2003). Previous section showed examples of anaemic galaxies, which very likely have experienced ram-pressure effects in the past, which led to significant gas deficiences in their disks. In this section we present observations of galaxies, which show clear evidence of recent perturbations exerted by the ICM. Two of them, NGC,4501 and NGC 4388 suffer heavy gas stripping and compressions, while the ISM of NGC 4535 seems to be moderately affected, though strong reaction of the magnetic field is observed.

Probably the most distinct example of a galaxy perturbed by ram-pressure stripping processes is NGC 4501 (Figs. 3.18 and 3.19). The asymmetry of the polarized emission is very high. About 75% of the emission comes from the southwestern side of the galaxy with respect to the major axis. It is hard to find such a distribution in normal galaxies. This may result from enhancements of regular and/or random anisotropic magnetic fields by compression. The details of such compression effects are described in Beck et al. (2005). If enhancements of the magnetic fields were the results of the compression in the sky plane, we would observe high polarization, what is the case. However, that does not mean we are observing highly ordered magnetic field, because such effect can be caused by either unidirectional or anisotropic random magnetic fields. As mentioned in Sect. 1.1, only Faraday rotation data can provide details about the coherence of the observed magnetic field and thus discriminate between pseudo-regular and regular magnetic fields. Our Faraday rotation data suggests that the magnetic field is coherent (Fig. 3.20), however this needs a confirmation with a higher resolution.

Our beam is too large to say definitely that we see a narrow compressional front in the highest polarized intensity region, however higher resolution VLA data of Vollmer et al. (2007) seem to confirm our suggestions. There are also a few more facts that seem to sustain this interpretation. The maximum of the polarized flux density occurs on the disk side where strong gradients of H I distribution are observed (Cayatte et al. 1990). Moreover, the optical structure also shows a smaller pitch angle on this disk side than on the opposite side. This asymmetry resembles that in NGC 4254, in which compression effects are suggested (Chyży et al. 2008). The explanation of the asymmetry of NGC 4501 by ram pressure stripping is supported by its quite high H I deficiency (see Table 4.12).

Also our X-ray data show that the emission from the hot gas in the nearest surroundings of the galaxy is distributed in a way that suggest a rapid movement through the ICM, with a visible gradient in the southwestern side and faint tails on the opposite side (Fig. 3.21), which is even more distinctly visible in the wide field low resolution image (Fig. 3.22). Unfortunately, the data is not sensitive enough to perform a detailed spectral analysis which would provide us with gas temperatures. This might definitely confirm compression and heating of the galaxy ISM. Therefore, obtaining a sensitive X-ray data for this galaxy seems is crucial.

The H I data by Cayatte et al. (1990) indicate that the northwestern half of the disk of NGC 4501 is approaching us. If the spiral is trailing this would mean that the compressed edge is the remote one and the galaxy is viewed "from below" (see also Onodera et al. 2004). The compression along the remote edge agrees well with a high positive velocity of NGC 4501 with respect to M 87 and to the average velocity for other galaxies in this Virgo Cluster region (Paturel et al. 2003). The galaxy though gas deficient is still forming stars at a reasonable rate, having B-V colour of $0^{\mathrm{m}}\!.62$ (see Table 4.11), which is a typical value for a galaxy of this morphological type and also finds confirmation in relatively low thermal fraction (see Table 4.12). On the other hand, U-B colour of $0^{\mathrm{m}}\!.26$ redder than for a normal galaxy suggests some deficiency of the youngest stars, thus slowering of the star formation. Surprisingly, this can also support the scenario of a strong compression that the galaxy is experiencing. Compression of the ISM of the galaxy may have improved to some extent the star forming activity which in turn sustained the magnetic field. This, of course could work until significant gas deficiency produced by heavy stripping has been reached. Magnetic field in NGC 4501 has the strength of the order of $10\,\mu$G, which is a typical value for a normal spiral galaxy (Niklas et al. 1997). We may therefore conclude that ram-pressure stripping effects may sustain strong magnetic fields in galaxies even highly deficient in gas.

Another global asymmetry of the magnetic field show the observations of an edge-on galaxy NGC 4388 (Figs. 3.10 and 3.11). The emission looks slightly shifted to the eastern side of this galaxy. Although it is not distinct in our observations due to a large beam, similar asymmetry was found by Vollmer et al. (2007). His high resolution observations show a complex structure of the magnetic field, however, due to possible missing flux they do not allow to study global asymmetries. Our observations, though of lower resolution show the overall properties of the magnetic field, such as its global inclination to the galactic plane. The asymmetry of the polarized intensity with higher polarization degree in the south and apparent polarization B-vectors aligned in the southeast-northwest direction suggest that the galaxy is moving in the southwestern direction, just as concluded by Yoshida et al. (2004) from Hα outflows alignment and their spectral analysis. This also seems to be confirmed by the archive X-ray data, where an extended hot gas tail is visible, as well as a significant gradient of the emission intensity in the southwestern part of the disk (Fig. 3.12). The galaxy shows quite low star formation rate, though significantly low thermal fraction (see Table 4.12). It might be however caused by an active nucleus of the galaxy contributing to the nonthermal emission. Calculations of the strength of the magnetic field were performed after the contribution form the active nucleus had been excluded. Although the total magnetic field strength of 6.6$\pm$2.1 μG is similar to that in NGC 4548 (6.3$\pm$1.8 μG), the regular component is a few times weaker and has a strength of 0.4$\pm$0.2 μG compared to 2.1$\pm$0.9 μG in NGC 4548. This may be the result of significant turbulence in the galactic medium introduced by stripping effects. It could be also caused by the beam depolarization, as the galaxy is comparable in size with the beam, however similar ratio is found for NGC 4548 as well.

Though seen from different angles, both NGC 4501 and NGC 4388 show some suggestions, that we might observe the same mechanism of intense ram-pressure stripping. The difference in gas abundance parameters and magnetic field strengths may lead to the conclusion that we are witnessing the same path of galactic evolution, though seen at two different stages. The distance to the cluster core of both galaxies also match such scenario. It is likely that in a few hundreds of Myrs the progressing stripping of NGC 4501 would lead to what we observe in the case of NGC 4388, which is nearly devoid of a gaseous disk and have much weaker magnetic fields. It is possible that in some time from now, after the stripping is ceased, both NGC 4388 and NGC 4501 would become similarly anaemic galaxies as NGC 4548 is at present.

Another example of ram pressure effects can be seen in the observations of NGC 4535 (Figs. 3.23, 3.25, and 3.24), though in this case the galaxy shows no distortions in neither the distribution of stars nor in neutral gas. Also the gas deficiency in this galaxy is rather moderate (see Table 4.11). Nevertheless, the peak of polarized intensity is located in only one optical spiral arm, while the total power emission is as symmetric, as the optical structure. The asymmetry in the distribution of polarized intensity, with over 70% of the emission coming from the western side, is clearly caused by an east-west gradient in the degree of magnetic field ordering, from 15% in the east to 40% in the west. This asymmetry is surprising because NGC 4535 is located in the southern Virgo extension (Böhringer et al. 1994), where the intracluster gas density is rather moderate. However, Otmianowska-Mazur & Vollmer (2003) show that the magnetic perturbations in the outer disk may last several hundred Myr after the passage through the dense ICM. Therefore, we cannot exclude the possibility that the observed distortions may have occurred in the past and are still visible. In this case strong magnetic anomalies accompanying only weak perturbations observed in the H I gas (Cayatte et al. 1990) may imply that the magnetic fields provide a very long-lasting memory of past interactions. Furthermore, the case of this galaxy could indicate that we can find highly compressed magnetic fields in galaxies far away from the cluster centre, where present-day ram pressure effects should be rather weak because of the expected lower ICM density. Despite the apparent compression of the magnetic field, both total and regular magnetic fields show rather moderate strengths of $8{\pm}2.4\,\mu$G and $2.5{\pm}1.1$, respectively.

A comparison of NGC 4501 and NGC 4535 shows pronounced differences. Although both galaxies seem to experience strong compression of their magnetic fields, only NGC 4501 has a magnetic field of a typical strength for a spiral galaxy ($\simeq$10 μG), having significant gas deficiency at the same time. This may be the result of differences in morphologies of both galaxies. NGC 4501 is a flocculent galaxy and therefore sensitive to gas dynamics and external influence. Significant compressions, visible in both optical and radio images, would allow the galaxy to keep normal level of the star formation despite gas removal in the course of ram-pressure stripping. As a result also the magnetic field strength could be sustained at a level typical for normal spiral galaxies. The optical structure of NGC 4535 and its dynamics is driven by an internal potential asymmetry associated with a bar, therefore, the galaxy is less sensitive for external influence. We may then conclude that such influence, clearly visible in our radio polarization data, can lead to strong magnetic field compressions, but may have no significant impact on the galaxy as a whole. Hence lower star formation of this moderately gas deficient galaxy and consequently lower magnetic field strength. Still, why the compression alone does not influence the strength of the magnetic field, especially its regular component, remains unanswered.

4.3 Tidal interactions

In the cluster environment gravitational encounters between galaxies are likely to be of high importance in the evolution of spiral galaxies. The spatial density of these object is much higher than of field galaxies. Nevertheless, such interactions do not necessarily lead to the total disrutpion of galaxies, as their high velocities allow the encounters to be relatively short. It was shown by numerical simulations (Soida et al. 2006, Vollmer et al. 2005), that typical timescales of developing tidal interaction signatures vary from 500 Myr in the Virgo Cluster outskirts to some 150 Myr near the cluster centre, as galactic velocities are higher towards the core. Though short, such gravitational effects may be strong and result in higher nuclear activity (LINER, Seyfert-type or nuclear starburst) triggered by distorted gas motions within the galaxy. Not only the general stellar structure can be affected, but also the gaseous disk and the magnetic field structure may be distorted producing outflows in a form of magnetized gaseous tails seen extending up to significant distances from the galaxy. We suggest such scenario in case of NGC 4438, with highly distorted optical structure and significant radio asymmetry. Also the observations in CO (Combes et al. 1988, Vollmer et al.2005) clearly suggest tidal interactions. Until recently it was believed that responsible for such distortions is the companion galaxy NGC 4435. However, lack of clear signs of distortions or gas deficiency in the mentioned galaxy raised doubts. Recent Hα observations of Kenney et al. (2008) showed between NGC 4438 and M 86 a long bridge of Hα emission, which suggests that the perturbations of NGC 4438 are likely caused by the past collision with M 86. Such scenario can be confirmed by X-ray archive observations of NGC 4438 and of the eastern parts of M 86 hot gas halo (Figs. 3.16 and 3.17). Hot gas in the vicinity of NGC 4438 and in the outer parts of M 86 (see Fig. 4.6) have similar temperatures (see Table 4.5), which may suggest that the gas could have been heated by the same process.

NGC 4438 shows a strong central source; it is an Sa type galaxy so it has a strong central mass concentration. Interferometric radio observations of Hummel & Saikia (1991) show that about 30% of the total flux density at 4.86 GHz comes from a compact radio shell surrounding the nucleus, classified in the NED database as a LINER. They also detected radio extensions, likely jets, up to $10''$, perpendicular to the galaxy plane. Such a nuclear activity can possibly be triggered by tidal influence (see above). Our observations also reveal a strong total intensity peak at the position of the galaxy centre (Fig. 3.14). The emission detected by Hummel & Saikia from all the structures in the galaxy centre accounts up to 58% of the total galaxy flux density detected in our single dish data. Fitting to the X-ray emission from the nucleus region (region 1 in Fig. 4.4) a model of a single temperature thermal plasma and a power law yields temperature of 0.67 ± 0.03 keV and a photon index of $1.18^{+0.20}_{-0.25}$ (see Table 4.3). High temperature in the central region also is a sign of an intense nuclear activity of NGC 4438. Our results for the nuclear region are with a good agreement with those obtained by Machacek et al. (2004).

With the high sensitivity to extended structures our polarization map also reveals weak extended emission on both sides of the disk much further, at least $3'$ (Sect. 3.5). These polarized features have an integrated intensity of

1.1±0.1 mJy and are associated neither with optical filaments nor with known background sources. As we checked, it is unlikely to be an instrumental effect, which is lower by almost one order of magnitude. The magnetic field vectors here have different orientation than in the disk or in the strong western extension, and are highly inclined to the disk. This may suggest that the vertical structures observed by Hummel & Saikia (1991) in the inner galaxy part continue as outflows up to 15 kpc from the disk. Such outflows must have a pressure and energy density high enough to overcome the ram pressure in the surrounding cluster medium.

In the small radio map ($20''$) in Hummel & Saikia the polarized peak seen in our single dish observations, is no longer visible, as it is shifted by almost $1'$ westwards from the centre in our data. Our resolution is too low to determine the origin of this shift. However, the "maximum subtraction method" (Chyży et al. 2003) reveals a strong total power residual (peak of $\approx$ 15 mJy/b.a.) southwest of the nucleus, which is roughly coincident with the polarized blob (Fig. 4.3). We checked that it is not due to a (possibly) non-Gaussian Effelsberg beam, and is not a sidelobe effect. A residual total power peak has been found in the same place by Kotanyi & Ekers (1983) who claimed it to be either due to external compression or tidal interactions. Our residual source is thus real, polarized with apparent polarization B-vectors parallel to the disk, and may be associated with extraplanar dust, Hα and X-ray structures. An impressive blob of polarized emission at this position visible in high resolution observations of Vollmer et al. (2007) confirms that. The tidal processes could stretch the magnetic field causing its amplification and thus enhancement of the polarized emission. Such case is likely observed in NGC 4254 (see Chyży et al. 2008). The tidal influence upon NGC 4438 could also align magnetic fields with extraplanar optical filaments parallel to the disk.

Our X-ray data (Fig. 3.16) show hot gas outflows emerging from the centre of the galaxy towards west and southwest. These features are on the same side of the disk as the region of the highest polarized emission visible in Fig. 3.15 and could also be attributed to tidal effects. The emission from the region west of the nucleus (region 2 in Fig. 4.4) can be best fitted with a single temperature thermal plasma and a power law, yielding gas temperature of 0.58±0.05 keV and photon index of 2.1±0.2 (Table 4.3). Weaker emission from the gaseous tail (region 3 in Fig. 4.4) was possible to fit only with a model of two temperature plasma and a power law, which yielded temperatures of $0.22^{+0.08}_{-0.04}$ keV and $0.65^{+0.07}_{-0.06}$ keV with 60% of the flux in the hotter component. The photon index of the power law component is $2.25^{+0.23}_{-0.25}$ (Table 4.3). Limited sensitivity of archive data does not allow to determine, whether the second thermal component in the fit to the region 3 is needed

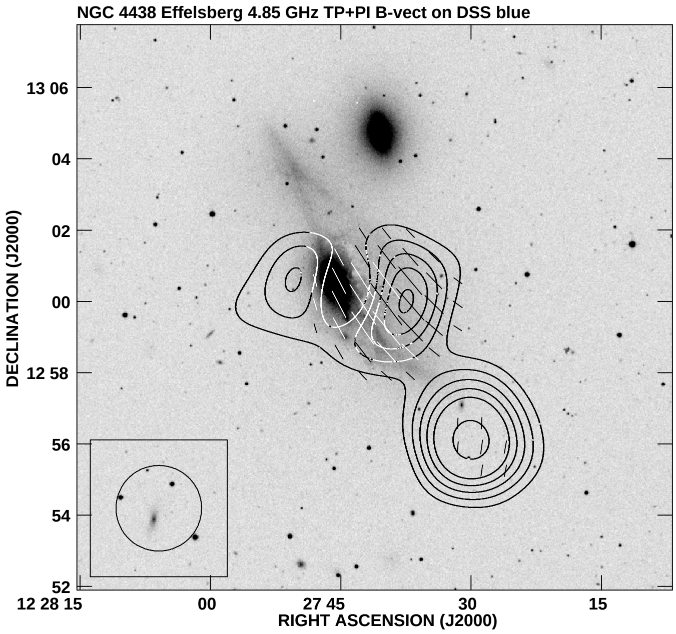

Figure 4.3: The residual total power brightness after the "maximum subtraction" of the central source with apparent polarization B-vectors for the brightest polarized peak, both overlaid onto the blue DSS image. The contour levels are 6, 9, 12, 15, 18, 25 $\times$ 0.7 mJy/b.a., and the polarization vectors are truncated at the level of 0.5 mJy/b.a.

due to low counts, and therefore to improve the quality of the fit, or it shows some contribution from the hot ICM in the gaseous tail. Such high temperatures of gas flowing out of NGC 4438, comparable to the temperature of the plasma in the nuclear region, can easily support the tidal interaction scenario, when hot gas is pulled out from the inner parts of the galaxy.

The wide field low-resolution (though more sensitive for faint extended structures) map (Fig. 3.17) shows, that between NGC 4438 and M 86 one giant halo-like brigde can be seen. This observation adds an important evidence to the scenario proposed by Kenney et al. (2008). They argue that it is impossible for an elliptic galaxy like M 86 to have such extended X-ray halo originally. It must have been formed after close passage (collision) with another galaxy, which most likely was NGC 4438. Our observations show that indeed, NGC 4438 is embedded in this halo, which seem to prove past interactions with M 86.

Although the archive data are not very sensitive, we made an attempt to examine the halo regions in order to look for signatures of interactions between both galaxies, which could be noticed as an additional thermal component in the fits of the hot ICM, which we also tried to detect. Therefore, for regions 4 through 8 we performed fits of the model consisting of two thermal plasmas, for the possible contribution from galactic gas and for the hot ICM, respectively, and a power law component for the emission from undetected point sources. Obtained parameters of this model are presented in Table 4.5 and calculated fluxes in Table 4.6.

The region south of NGC 4438 (region 4 in Fig. 4.6) fitted with two temperature model yielded unphysical results. Fitting single temperature model yielded a temperature of $1.63^{+0.23}_{-0.25}$ keV (see Table 4.5), which high value can be associated with the emission from the hot ICM, as the region is situated outside of the galaxy. Still, much of the emission comes from the power law component (Table 4.6), which can be attributed to background sources. For the region 5 (see Fig. 4.6), which is also outside of NGC 4438 but at the same in the direction to M 86, it was possible to perform a two temperature fit. We obtained temperatures of $0.77^{+0.06}_{-0.08}$ keV and $2.32^{+0.33}_{-0.30}$ keV, respectively (Table 4.5). It is possible that the cooler component can be atrributed to the hot gas originating in tidal interactions between NGC 4438 and M 86, and the hot component to the ICM, however, more sensitive data should be analysed to confirm such results. Especially, that the hotter component temperature is marked with significant uncertainties. Nevertheless, temperature of the ICM of the order of 2 keV is consistent with those obtained by Shibata et al. (2001) for this region of the Virgo Cluster. Temperatures of the cooler gas component of the order of 0.75 keV we can find also in regions 6 and 7 (Fig. 4.6), which could support the existence of the gas from both galaxies in the hot gas halo of M 86 and thus add another evidence for their past interaction. Temperatures of hot gas components of regions 6 and 7 are of the order of 1.7 keV, which also seems to correspond with the region 5, within errors. Nevertheless, we could expect the ICM to be slightly cooler in the neighbourhood of M 86 due to mixing with its halo. Also the relative abundance of cool and hot components in regions 6 and 7 is in an agreement with the proposed tidal interaction scenario. The contribution from the cool gas (possibly originated in the interaction) drops from 49% in the region 6 to 22% in the region 7. It is therefore justified to fit the most distant region 8 only with single temperature plasma, as we could expect a contribution only from the ICM, which also seems to be justified by its significant distance to both NGC 4438 and M 86 (cf. Fig. 4.6). The obtained temperature of $2.16^{+0.57}_{-0.38}$ keV, though marked with significant uncertainties, is with an agreement with analysis of Shibata et al. (2001), especially that this region can be also influenced by the halo of M 87, which is some $40'$ (around 200 kpc in the sky plane) southeast from the eastern edge of the field of view in Fig. 4.6.

What is even more interesting, also another galaxy, NGC 4388, could play some part in this scenario, as its hot gas tail is extending towards the halo of M 86, reaching almost the position of the Hα bridge (see Figs. 3.13 and 3.17). Yoshida et al. (2004) argue that an Hα tail of NGC 4388 is produced by the ionisation of the expelled matter by the active nucleus of this galaxy. Its origin however could probably be also linked with tidal interactions with M 86. Although its velocity is high and could prevent the galaxy from tidal interactions (Kenney et al. 2008), one cannot definitely exclude such possibility.

Our findings from X-ray data once again seem to confirm that past tidal interactions between M 86 and NGC 4438 are the most likely scenario to explain the observed features. Similarly to what we concluded from the observations of heavily stripped galaxies affected by the ram-pressure effects, also here we see a galaxy NGC 4438 which became highly gas deficient, but this time it was due to losses suffered from tidal encounters. Magnetic field strengths ($3.9\pm1.3\,\mu$G and $0.6\pm0.3\,\mu$G for the total and the regular magnetic field, respectively) of this galaxy calculated from our data (see Table 4.12) are typical rather for low mass, weakly forming stars dwarf galaxies (Chyży et al. in prep.).

Although limited in sensitivity, the archive data for NGC 4438 and M 86 provide some possibilities to trace signs of their past interactions. More sensitive data would definitely allow to verify the above results and possibly provide better determinations of the fit parameters. A thorough study of the whole region of M 86 and M 87, especially of NGC 4438 and NGC 4388 are needed to provide more clues on the past and present evolution of this intriquing part of the Virgo Cluster.

Table 4.3: Model fit parameters of selected regions in NGC 4438

Reg. no.	kT_1 [keV]	kT_2 [keV]	Photon Index
1	0.67 ± 0.03	–	$1.18^{+0.20}_{-0.25}$
2	0.58 ± 0.05	–	2.1 ± 0.2
3	$0.22^{+0.08}_{-0.04}$	$0.65^{+0.07}_{-0.06}$	$2.25^{+0.23}_{-0.25}$

Another case of tidally interacting galaxies are most likely NGC 4302 and NGC 4298, though lack of visible perturbations of their disk suggests that the encounter is just starting. The eastern extension from NGC 4302

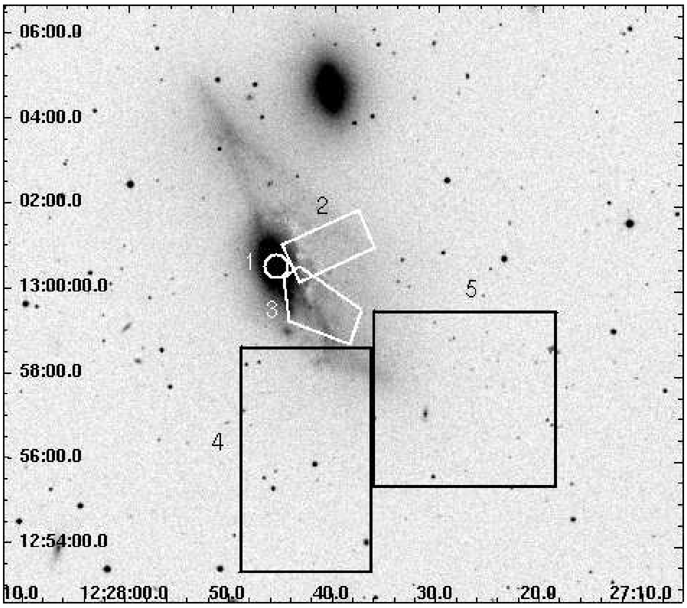

Figure 4.4: Regions of NGC 4438 and the surroundings for which the spectra were aquired. All background sources were extracted before creating the spectrum.

up to 2′ (10 kpc in the sky plane) followed by apparent polarization B-vectors together with peak of polarized intensity shifted towards NGC 4298 may suggest that both galaxies constitute a physical pair, especially as their difference in radial velocities is only about 14 km/s. Most of the polarized emission is located in the region between the galaxies, where the highest polarization degree is observed. Our beam is however too large to investigate the magnetic fields of NGC 4302 and NGC 4298 in more detail. Nevertheless, we can still expect that there is a region of compressed magnetic field *between* NGC 4302 and NGC 4298 resembling that in NGC 4038/4039 system (Chyży & Beck 2004), especially that the degree of polarization is higher in the region between NGC 4298 and NGC 4302 and reaches ≃15% compared to ≃10% in the region between NGC 4038 and NGC 4039. High resolution polarimetric observations of NGC 4302 and NGC 4298 are desirable, especially of the latter one, since with our large beam we cannot detect polarized intensity due to beam depolarization effects. The calculation of the magnetic field strengths is also difficult, only at 8.35 GHz, where the emission is weaker, it was possible to resolve both galaxies. We obtained values of $8.9 \pm 2.7\,\mu$G and $7.7 \pm 2.5\,\mu$G for total magnetic field strengths for NGC 4298 and NGC 4302, respectively (see Table 4.12), which are rather moderate for normal spiral galaxies.

Table 4.4: 0.2 - 12 keV unabsorbed fluxes in erg $cm^{-2}s^{-1}$ for modelled regions in NGC 4438.

Reg. no.	mekal 1	mekal 2	powerlaw	total
1*	1.12e-13	–	2.51e-13	3.63e-13
2	6.19e-14	–	1.39e-13	2.01e-13
3	3.05e-14	5.17e-14	1.25e-13	2.07e-13

* Due to bad data above 10 keV fluxes are derived in the band 0.2 - 10 keV.

Table 4.5: Model fit parameters of M 86 halo regions.

Reg. no.	kT_1 [keV]	kT_2 [keV]	Pho Index
4	$1.63^{+0.23}_{-0.25}$	–	$1.93^{+0.10}_{-0.08}$
5	$0.77^{+0.06}_{-0.08}$	$2.32^{+0.33}_{-0.30}$	$2.32^{+0.21}_{-0.19}$
6	$0.72^{+0.03}_{-0.02}$	$1.62^{+0.18}_{-0.20}$	$2.46^{+1.06}_{-0.39}$
7	0.78 ± 0.06	$1.8^{+0.41}_{-0.17}$	$2.08^{+0.17}_{-0.08}$
8	$2.16^{+0.57}_{-0.38}$	–	$1.95^{+0.17}_{-0.08}$

Chung et al. (2007) reported a mild truncation of the H I disk of NGC 4302 together with gas tail extending to the north. There is also a shift visible between H I and stellar disk of NGC 4298. They found no significant neutral hydrogen emission between both galaxies. Koopmann et al. (2004) discovered in NGC 4298 asymmetric Hα extensions on the side closest to NGC 4302, as well as asymmetric red light morphology. In addition, Heald et al. (2007) examined warm diffuse ionized gas halo around NGC 4302, which possibly can be caused by an increased central activity induced by the companion galaxy. Similarly, a weak X-ray emission visible between NGC 4302 and NGC 4298, suggesting a gaseous bridge, can also support the tidal interaction scenario. Distorted H I and Hα distributions, together with our radio polarization findings may provide sufficent evidences that we observe a physical pair of interacting galaxies. Just as the existence of an ULX source in the eastern side of NGC 4298, that can mark a region of intense star formation possibly triggered by galactic interactions, similarly to what we observe in

Table 4.6: 0.2 - 12 keV unabsorbed fluxes in erg $cm^{-2}s^{-1}$ for modelled regions in the outer halo of M 86.

Reg. no.	mekal 1	mekal 2	powerlaw	total
4	1.57e-13	–	7.05e-13	8.65e-13
5	8.65e-14	3.19e-13	2.48e-13	6.53e-13
6	9.43e-13	9.95e-13	3.23e-13	2.26e-12
7	3.27e-13	1.16e-12	1.91e-12	3.40e-12
8	6.42e-13	–	1.42e-12	2.06e-12

NGC 4254. To get more clues about the possible interactions between both galaxies we performed spectral analysis of our X-ray data, especially of the region between both galaxies. The disks of both galaxies were fitted with a single temperature thermal plasma with an addition from point sources well described by a power law spectrum. The fits yielded rather typical gas temperatures of the order of 0.2 keV, though in the disk of NGC 4302 the slope of the power law component is surprisingly "flat" for a contribution from expected undetected sources. Together with high contribution of this component to the total flux (87%) it might be another evidence of an increased activity of this galaxy, as argued above. Especially, that the gas temperature in this galaxy is slightly higher than in NGC 4298. It is however within the errors, as well as the temperatures of the features outside of the disks of both galaxies. In such case one cannot state definitely about the real differences without more sensitive data that could allow to perform spectral analysis resulting in well constrained parameters.

For the most interesting region of hot gas emission, the intergalactic region, the model of two temperature plasma was used due to overall weak emission resulting in low number of photons. The fit yielded the temperatures of 0.12 and 0.66 keV (see Table 4.7). This could suggest mixing and partial heating of the gas pulled out from both galaxies, provided the interactions take place. The contribution of the hotter component (16%) is low enough to state that in that case the interactions are at its early stage, what still would be consistent with observations in radio, H I, or Hα. If we consider all these observations to constitute one global picture of this pair of galaxies it seems highly probable that indeed we are seeing two galaxies at the beginning of their encounter.

Much more sensitive observations are however needed. Especially, that our observations were made using a medium filter which definitely lowered the sensitivity to the softest part of the data. Therefore, sensitive observations using the thin filter would likely improve our fits, as well as possibly allow to detect more emission from the diffuse gas in the region between galaxies.

Table 4.7: Model fit parameters of NGC 4298 and NGC 4302 regions.

Reg. no.	kT_1 [keV]	kT_2 [keV]	Photon Index
1	$0.2^{+0.13}_{-0.1}$	–	$2.1^{+0.25}_{-0.27}$
2	$0.21^{+0.12}_{-0.09}$	–	–
3	$0.23^{+0.07}_{-0.09}$	–	$1.35^{+0.40}_{-0.33}$
4	$0.19^{+0.14}_{-0.07}$	–	–
5	0.12 ± 0.03	$0.66^{+0.20}_{-0.28}$	–

Table 4.8: 0.2 - 12 keV unabsorbed fluxes in erg $cm^{-2}s^{-1}$ for modelled regions in NGC 4298 and NGC 4302.

Reg. no.	mekal 1	mekal 2	powerlaw	total
1	5.31e-15	–	5.73e-14	6.26e-14
2	2.16e-15	–	–	2.16e-15
3	4.44e-15	–	2.91e-14	3.35e-14
4	1.60e-15	–	–	1.60e-15
5	1.06e-14	2.03e-15	–	1.27e-14

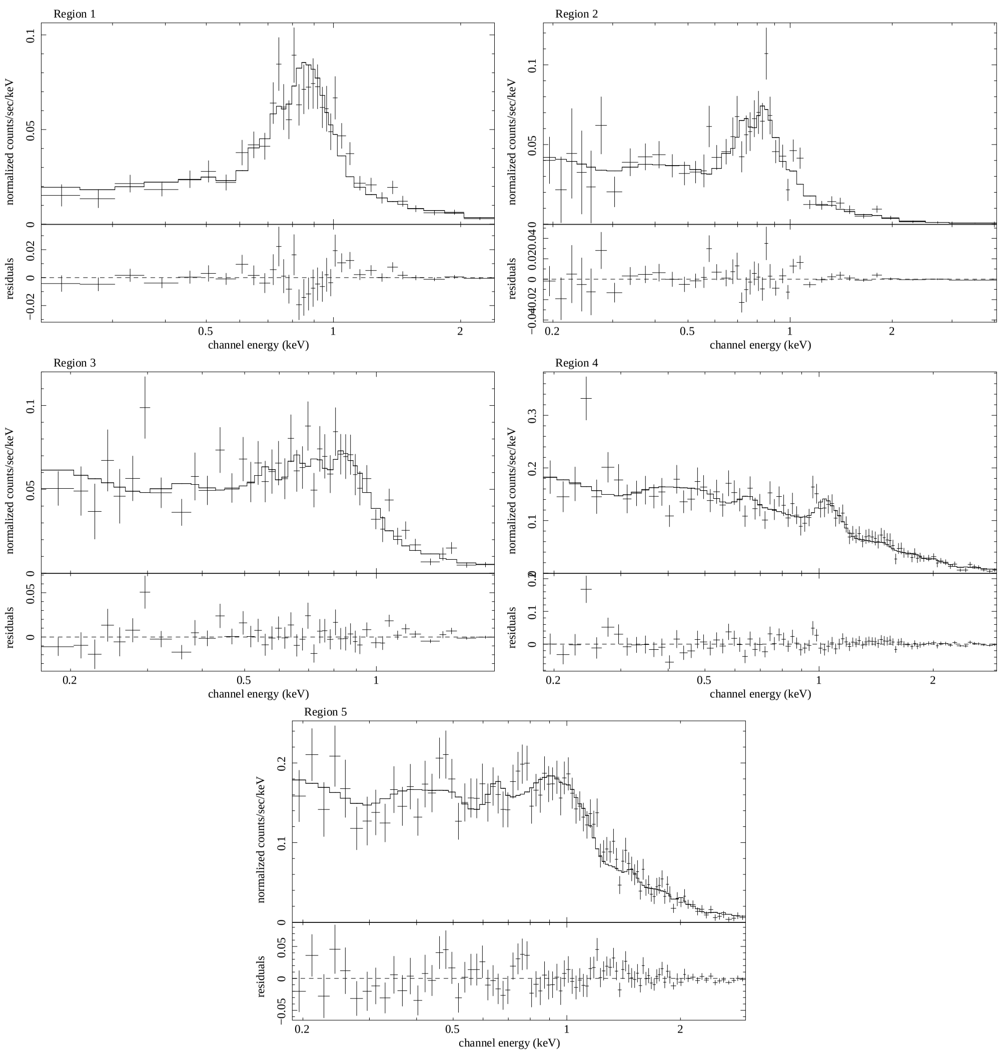

Figure 4.5: Model fits to the regions of NGC 4438. See tables 4.3 and 4.4.

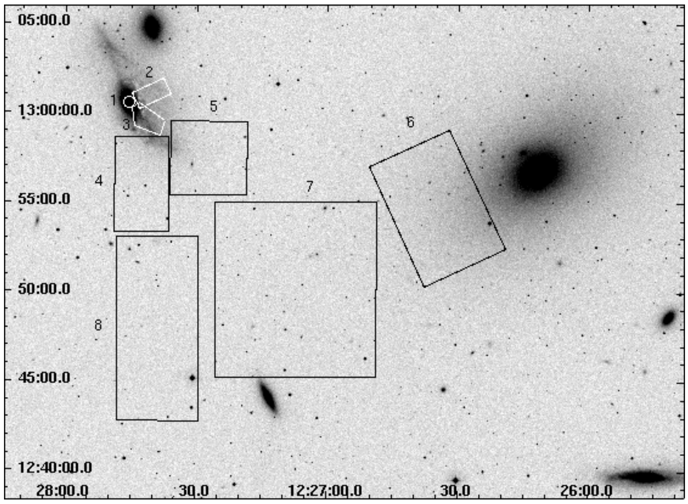

Figure 4.6: Regions of the halo of M 86 for which the spectra were aquired. All background sources were extracted before creating the spectrum.

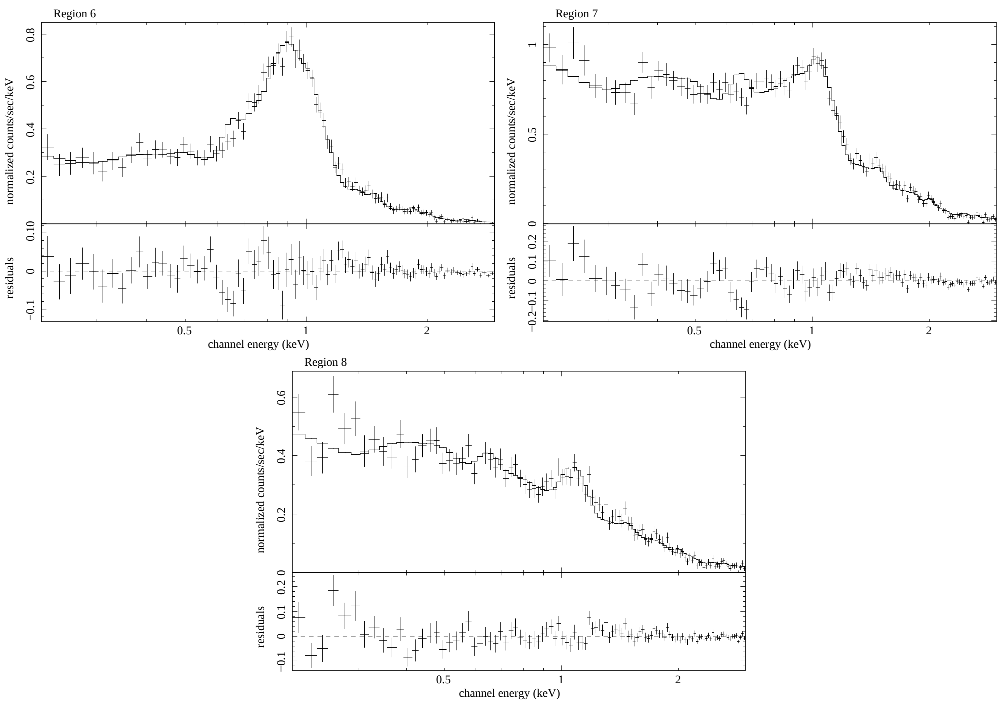

Figure 4.7: Model fits to the regions of M 86 halo. See tables 4.5 and 4.6.

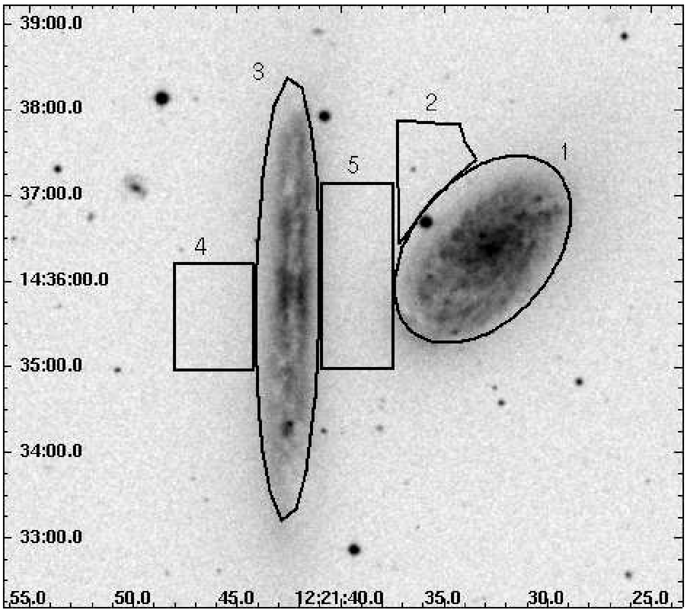

Figure 4.8: Spectral regions of NGC 4298 and NGC 4302 for which the spectra were aquired. All background sources were extracted before creating the spectrum.

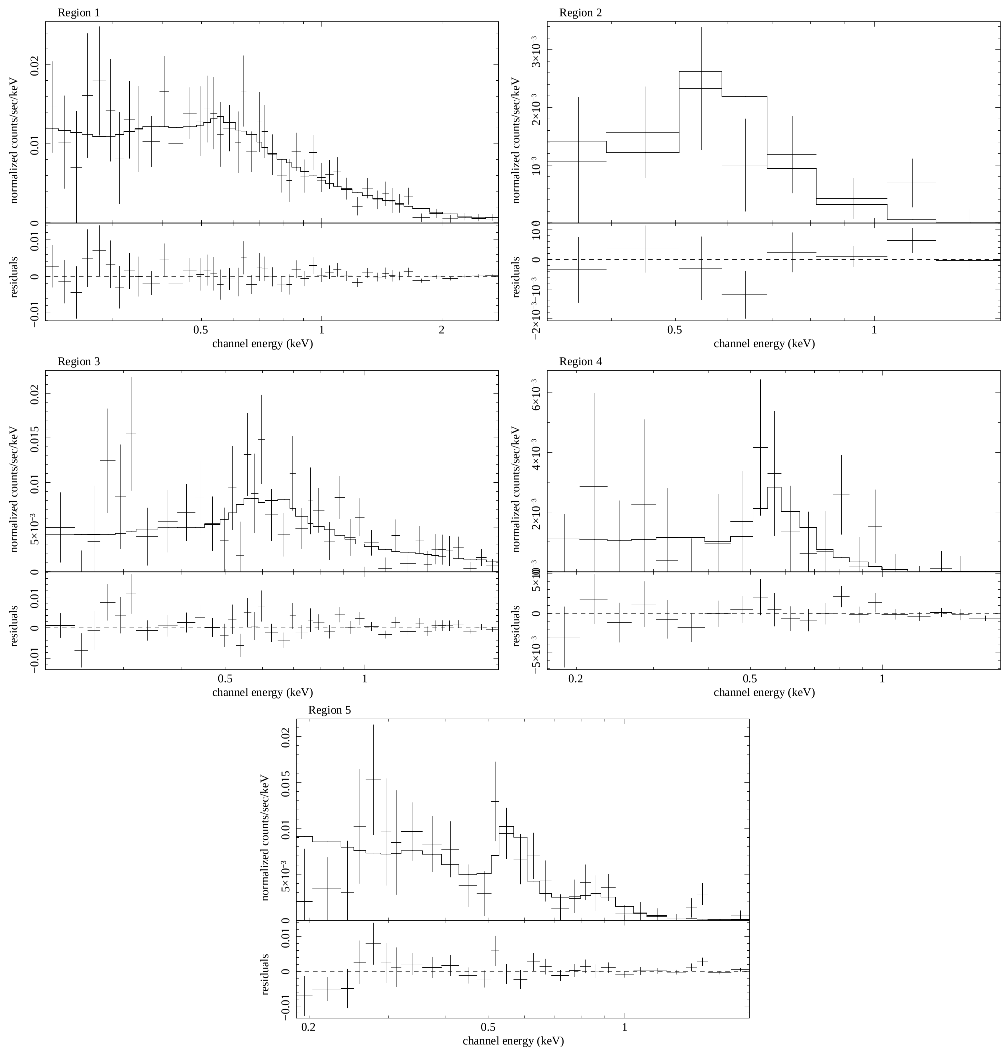

Figure 4.9: Model fits to the regions of NGC 4298 and NGC 4302. See tables 4.7 and 4.8.

4.4 Moderately affected galaxies

To obtain a global view of the disturbances originating in the cluster environment and its impact on both gaseous and star components, as well as its connection with magnetic properties, we studied also galaxies that are somewhat intermediate objects in the sample. In the preceding sections galaxies with high gas deficiency and/or significantly distorted were described. In this section two galaxies showing no significant gas deficiency and presenting a normal star formation level are discussed, with one of them being however significantly perturbed. It is NGC 4254, a tidally distorted galaxy but with a normal gas content. The second one, NGC 4321, is a moderately gas deficient galaxy, normally forming stars and showing no clear sings of any distortions.

NGC 4254 was thoroughly studied in the radio domain by Chyży (2008). The author argued that the distorted optical morphology and a region of bright polarized intensity visible in this galaxy are not caused by stripping effects but result from tidal interactions with the dark galaxy VIRGO HI 21 discovered by Minchin et al. (2007). The polarized ridge would be thus produced by pulling of the spiral arm out of the galaxy (northwards) and compressing the magnetic field in the southern part of the disk, where the rigde is visible (Chyży et al. 2008). Our X-ray observations of this galaxy confirm this argumentation. Although the gas distribution does not suggest any compressions or outflows, spectral analysis reveals more clues. Enough photon counts allowed all regions presented in Fig. 4.10 to be fitted with single temperature thermal plasma with an admixture of undetected point sources (power law). In case of the interarm region just the thermal plasma model without power law component was sufficient, as we do not expect significant contribution from galactic point sources away from star forming spiral arms. All three arms of the galaxy showed similar gas temperatures with only eastern arm slightly hotter. It could be easily explained by the existence of bright Hα clumps in this arm, which can contribute to the higher star formation and thus heating the surroundings in this region. The compression region, where the polarized rigde is visible has a similar temperature, what clearly shows we are not dealing with shock heating caused by a rapid movement of the galaxy through the hot ICM. The gas would be in such case heated significantly in comparison to the other parts of the galaxy (as in the case of NGC 4569 - see sect. 4.1). Especially, that the outer part of the compression region is even cooler. The galaxy is vividly forming stars and shows no gas deficiency, what results in a strong magnetic field of $16\pm1\,\mu$G (Chyży et al. 2007).

The opposite situation to NGC 4254 we see in case of NGC 4321. The gas deficiency in this galaxy is rather moderate (see Table 4.11) but the galaxy

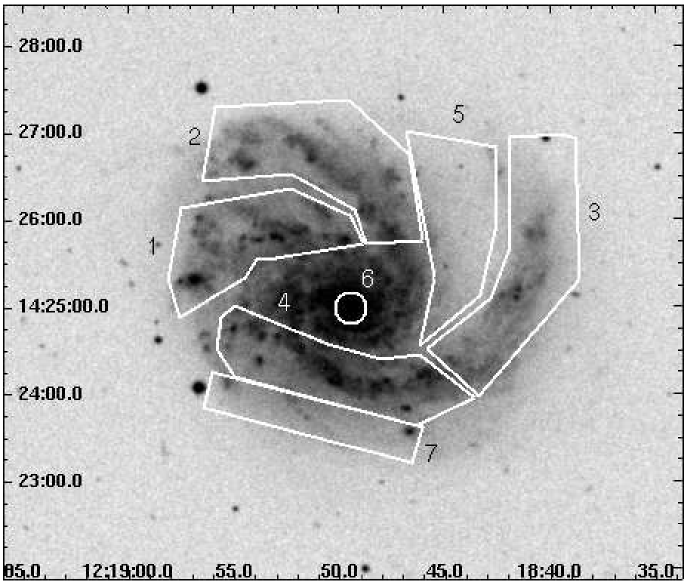

Figure 4.10: Spectral regions of NGC 4254 for which the spectra were aquired. All background sources were extracted before creating the spectrum.

shows no clear signs of interactions. What is a bit surprising, no ram-pressure stripping effects exerted upon its gaseous disk are visible, which could explain gas deficiency. However, one might note two features, an H I ridge and a faint H I tail placed on opposite sides of the disk (Knapen 1993). A lack of other significant distortions would suggest, that the galaxy is starting to experience that kind of interactions or that the perturbations are quite weak, which could be supported by a significant distance to the cluster centre, hence low density ICM. On the other hand, the tidal interactions scenario is also possible, as two companion galaxies are visible in the vicinity of NGC 4321. These are NGC 4322, $5.3'$ to the north, and NGC 4328, $6.1'$ to the east with a faint visible bridge connecting the latter to NGC 4321. Still, the total magnetic field strength and star formation rate in this galaxy are rather normal (11.3 ± 3.4 μG and 2.12 $M_{\odot}yr^{-1}$, respectively). This could mean, that gas deficiency in this galaxy is not directly related to its magnetic properties, which in turn may suggest that we are seeing early stages of the perturbances and the magnetic field still remains unaffected. We argue that this regularly-looking barred galaxy with homogenous H I distribution very likely is a relatively new member of the cluster.

Table 4.9: Model fit parameters of NGC 4254 regions.

Reg. no.	kT_1 [keV]	Photon Index
1	$0.41^{+0.18}_{-0.11}$	$2.15^{+0.21}_{-0.25}$
2	$0.28^{+0.58}_{-0.07}$	$2^{+0.65}_{-0.73}$
3	$0.33^{+0.13}_{-0.07}$	–
4	$0.30^{+0.02}_{-0.03}$	$1.92^{+0.27}_{-0.31}$
5	$0.27^{+0.07}_{-0.04}$	–
6	$0.53^{+0.22}_{-0.23}$	$2.62^{+0.43}_{-0.42}$
7	0.14 ± 0.04	$1.25^{+1.12}_{-1.60}$

Table 4.10: 0.2 - 12 keV unabsorbed fluxes in $\mathrm{erg\,cm^{-2}s^{-1}}$ for modelled regions in NGC 4254.

Reg. no.	mekal 1	powerlaw	total
1	1.49e-14	1.03e-13	1.18e-13
2	9.08e-15	2.63e-14	3.54e-14
3	1.42e-14	–	1.42e-14
4	6.04e-14	8.99e-14	1.50e-13
5	1.22e-14	–	1.22e-14
6*	7.06e-15	3.20e-14	3.90e-14
7	1.09e-14	2.85e-14	3.94e-14

* Due to data quality and low counts fluxes derived in the band 0.2 - 5.37 keV.

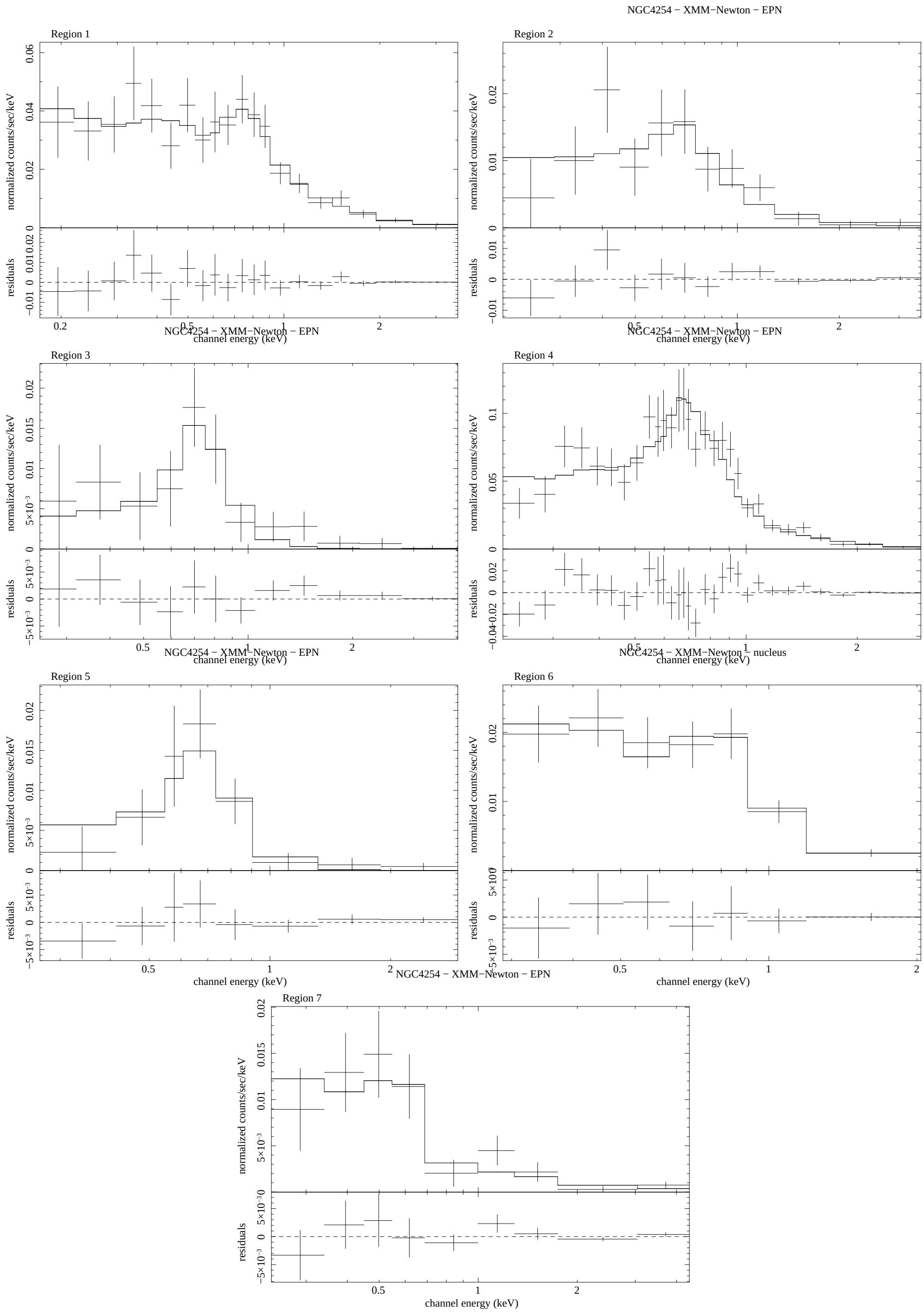

Figure 4.11: Model fits to the regions of NGC 4254. See tables 4.9 and 4.10.

4.5 Global properties of studied galaxies

In order to calculate magnetic field strengths for our sample galaxies it is neccessary to know which part of the total emission from a given galaxy is coming from the nonthermal component. To do that, one needs to derive the thermal fraction. The easiest approach is to use a typical value for spiral galaxies (see Niklas et al. 1997). However, in the case of our sample, the best would be to know precise values for each galaxy. Only then our computations could show any trends in the behaviour of gas deficient galaxies. Similarly, the nonthermal spectral index, also used in magnetic field strength calculation, should not be taken as an average value for field galaxies.

Investigations of the influence of the star formation conditions upon the magnetic properties require the derivation of thermal fractions in order to calculate the mean *nonthermal* emission which is associated with magnetic fields. The thermal fraction can be derived from either the Hα or the far infrared emission. Using Hα fluxes can be difficult, as their derivation requires corrections for galactic extinction and N II contamination, which are difficult to estimate. This can lead to significant uncertainties of the derived fluxes and subsequently to uncertain thermal fraction values. Calculations based on far-infrared fluxes are free from extinction influence, however, this method work best in the case of starburst galaxies (Kennicutt 1998). As this study concentrates on gas deficient galaxies, we can expect lower star formation rates for them. Taking all the above arguments under consideration we performed calculations of thermal fractions using both methods, which will allow to compare results and estimate their reliability.

Using Hα fluxes it is possible to calculate the thermal radio flux according to the following formula (Niklas et al. 1997):

$$\begin{aligned} S_t[mJy] = 2.238 \times 10^9 \cdot S_{H\alpha}[erg\,s^{-1}cm^{-2}] \cdot (T_e)^{0.42}[K] \times \\ \times \left(ln\left(\frac{0.04995}{\nu[GHz]}\right) + 1.5 \cdot ln(T_e)[K] \right), \end{aligned} \tag{4.1}$$

where T_e is electron temperature, here 10^4 K, and ν is the frequency, for which the thermal flux is being calculated. Dividing this flux by the observed radio flux we obtain the thermal fraction.

To calculate the total far infrared flux the following formula is used (Helou et al. 1985):

$$F_{FIR}[erg\,s^{-1}\,m^{-2}] = 1.26 \times 10^{-7} \cdot (2.58 F_{60\mu m}[Jy] + F_{100\mu m}[Jy]). \tag{4.2}$$

Now we use formulae provided by Kennicutt (1998). They connect Hα and far-infrared luminosity via star formation rates, hence we obtain the direct link between Hα and far-infrared fluxes:

$$S_{H\alpha}[erg\,s^{-1}cm^{-2}] = 5.7 \times 10^{-7} \cdot F_{FIR}[erg\,s^{-1}\,cm^{-2}], \tag{4.3}$$

Now, with Hα fluxes calculated form total far-infrared fluxes, we can follow the first method routine and calculate the thermal fractions relatively free from any absorption influence. Values obtained independently from both methods are in a good agreement, (see Table 4.11), which suggests that they are sufficiently reliable.

As mentioned above, we can also calculate star formation rates using independently Hα (Koopmann et al. 2001, Buat et al. 2002) and far-infrared (Helou et al. 1985) fluxes. All the values of thermal fractions and star formation rates obtained using both methods are summarized in Table 4.11.

To calculate nonthermal radio spectral indices we use the formula given by Niklas et al. (1997) and derive the expression for the nonthermal index:

$$\alpha_{nth} = -\frac{log\left[\frac{\frac{S_\nu}{S_{\nu_0}} - f_{th}(\nu_0)\left(\frac{\nu}{\nu_0}\right)^{-0.1}}{1-f_{th}(\nu_0)}\right]}{log\left(\frac{\nu}{\nu_0}\right)}. \tag{4.4}$$

This model assumes that the medium of the galaxy is optically thin and that the nonthermal spectral index is constant over the disk and frequency range. For our calculations we used 6 cm radio fluxes from this work, as well as VLA fluxes at 1.4 GHz (Soida priv. comm., except for NGC 4548, for which we used the 10.55 GHz radio flux from Niklas et al. 1997). In the case of NGC 4298 and NGC 4302 we used 3.6 cm fluxes, as this galaxy pair is unresolved at 6 cm.

Once we have derived thermal fractions and nonthermal indices, we can calculate the total, as well as regular magnetic field. The equipartition magnetic fields were computed from the nonthermal surface brightness (according to Beck & Krause 2005). We used the mean value of the nonthermal surface brightness at 4.85 GHz (8.35 GHz for NGC 4298 and NGC 4302), free from central source contribution in the case of NGC 4388 and NGC 4438, integrated over the optical disk and assumed a proton-to-electron ratio of 100. For a synchrotron face-on disk thickness a value of 1 kpc was assumed. For edge-on or nearly edge-on galaxies in our sample (NGC 4302, NGC 4388, and NGC 4438) the value corresponding to the integration along the whole disk (based on an apparent size of the disk at the assumed distance to the Virgo Cluster) was used. The integration over the optical disk was chosen in order to avoid beam smearing of the signal leading to lower surface-brightnessess, especially in egde-on galaxies, which disk thicknesses are smaller than our beam (2ʹ.5 at 4.85 GHz). Also in anaemic galaxies, which tend to show radio emission only from central parts of their disks, that kind of integration does not lead to overestimation of the surface-brightness. The resulting total and regular magnetic field strengths are presented at the end of this section in Table 4.12. Their errors include 50% uncertainties of the above parameter values.

To compare the integrated total power emission of the studied Virgo Cluster spirals to non-cluster nearby spiral galaxies we use the radio – far-infrared (FIR) correlation. The radio and FIR surface brightnesses are computed as the ratio of integrated flux density at 4.85 GHz and at 60μm to their face-on corrected observed disk surface. For that purpose we used the extinction-corrected diameters from the LEDA database (Paturel et al. 2003). As a homogenous comparison sample we took the galaxies measured at 4.8 GHz by Gioia et al. (1982) who used the same instrument and a similar method of integrating the total power flux density. The reference sample has been extended towards low intensities using the 4.85 GHz Effelsberg measurements of slowly star forming galaxies (Chyży et al. 2007).

The radio-FIR correlation for our Virgo sample and the comparison sample is shown in Fig. 4.12. Four normally star-forming galaxies NGC 4254, NGC 4321, NGC 4501 and NGC 4535 closely follow the relation derived for non-Virgo spirals, which has a slope of 0.96±0.06. NGC 4438 is placed considerably above this relation.

The excess could be due to either the western polarized radio peak (Fig. 4.3), probably associated with some extraplanar radio emission (Kotanyi & Ekers 1983), or to nonthermal structures unrelated to star formation originating in the nuclear region. According to the VLA map at 4.85 GHz by Vollmer et al. (2007) the central region of NGC 4438 contributes less than 50% to the total flux density at 4.85 GHz while the images from the ISO archive show this region to be the source of the bulk of FIR emission. On the other hand the extraplanar radio source of Kotanyi & Ekers (1983) emitting much less in FIR amounts to only some 10 – 12% of the total flux at 1.4 GHz, probably the same fraction at 4.85 GHz. All this is too little for an excess by a factor of 5, thus there should be another component undetected by interferometers and not related to star formation, contributing to the excess of radio over FIR emission. To establish a possible association of the excess with circumnuclear or extraplanar structures or to say whether we are dealing with compressional enhancement of magnetic fields as proposed by Reddy & Yun (2004) we need a substantially better resolution with enough sensitivity to extended structures. We note finally that a similar excess of radio over FIR emission for cluster spirals has been noted by Gavazzi (1998).

NGC 4388, a heavily stripped galaxy, does not deviate above the correlation as much, as in the case of NGC 4438, though the radio excess is clearly visible. This highly gas-deficient galaxy also possesses an active nucleus (Seyfert 2), which may contribute to the radio emission regardless of gas abundance and star formation. Such enhanced nonthermal radio emission is also confirmed by extremely low thermal fraction of NGC 4388 (and NGC 4438 as well – see Table 4.11). The opposite situation is in the case of NGC 4548, which is even more gas deficient and shows some deficit of the radio emission. This can be however by the fact that NGC 4548 is an anaemic galaxy and has a radio surface brightness lower than any galaxy in the sample of Gioia et al. (1982). It also belongs to the weakest FIR emitters in that sample, the weak radio emission is therefore largely due to a low star formation level.

For a comparison, another anaemic galaxy, but hosting an active nucleus, NGC 4579, has been included in the correlation. It shows an excess of radio emission, but with the central source excluded the galaxy follows well the correlation. It is therefore worth noticing that galaxies suspected for hosting an active nucleus are generally situated above the correlation line and show very low thermal fractions, at the same time. This can be explained by additional nonthermal emission from the nuclear region, unrelated to star formation and thus producing less far-infrared emission. When excluding central sources, also those galaxies follow the correlation. Three remaining galaxies, NGC 4569 and NGC 4302 together with NGC 4298 do not deviate from the correlation by more than the dispersion for comparison sample galaxies.

Previous sections suggest that all gas deficient or perturbed galaxies have magnetic fields of rather moderate strength. However, compression effects are likely capable of amplifying the total magnetic field of a gas deficient galaxy to the values of normal spirals (around 10%, see Niklas et al. 1997), as we probably see in the case of NGC 4501. In this galaxy we also see an increase in the regularity of the magnetic field, which should be no surprising, as the galaxy experiences heavy compression of the leading side of the disk. It is however the question, to what extent can such effects amplify magnetic fields. More observations of galaxies of the same morphological type and similar gas deficiency should be performed to estimate the efficiency of this phenomenon. It is possible that only when the galaxy is perturbed on shorter timescales, the magnetic field can be amplified during gas losses experienced by a galaxy. If distortions are produced at a slow rate, gas losses would be more significant that the amplification of magnetic fields on longer timescales. On the other hand, we might by seeing simply different stages of the perturbing processes.

NGC 4501 could be a galaxy that has been perturbed for a relatively short time, which could be possible regarding its rapid movement. In such case resulting strong compressions would sustain significant magnetic fields. The supporting arguments for such scenarios provide the observations of quite normal galaxies like NGC 4321, which seems to be an example of a galaxy that is gas deficient, hovewer lacks any signs of strong perturbations. It may suggests that the H I gas has been or still is being removed slowly, which in turn leads to a conclusion, that the magnetic field in such case could be sustained at a normal level still for some time, what is observed.

Only NGC 4535 doesn't fit such scenario. Slightly weaker than typical total magnetic field can be easily explained by moderate gas deficiency leading to lower star formation. Its magnetic field is however strongly compressed on the western side, which should lead to its amplification, especially of the regular component, as seen in the case of NGC 4501. Why we do not see such enhancement of the magnetic field is a question.

A larger sample of gas deficient and/or perturbed galaxies are desirable to further study the influence of the distortions on the evolution of the magnetic fields.

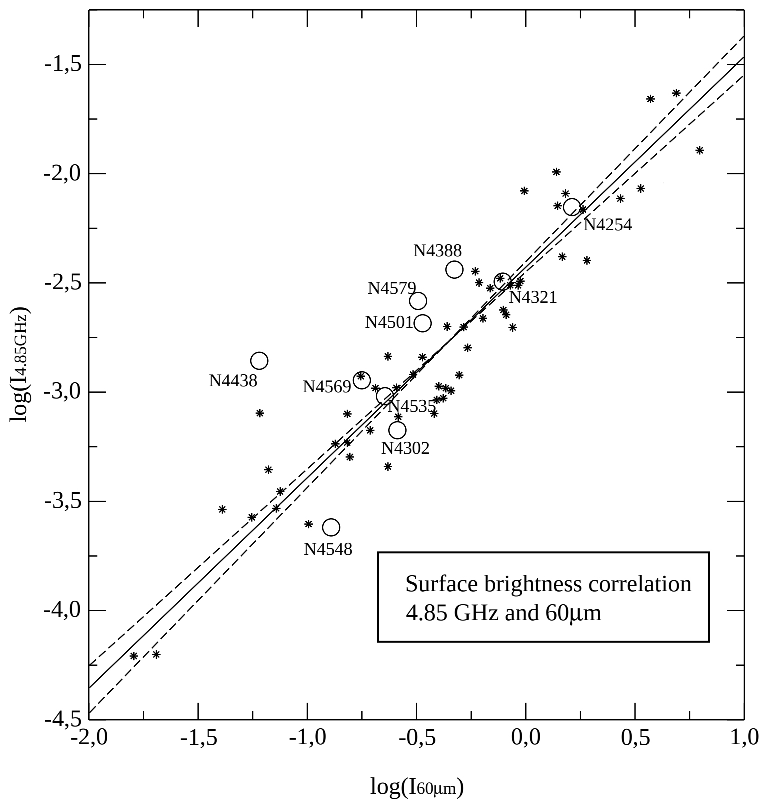

Figure 4.12: The radio - FIR correlation diagram for our Virgo objects plotted as symbols with labels and for the reference sample of galaxies observed by Gioia et al. (1982) with an extension towards low-surface brightness objects observed by Chyży et al. (2007) – both as dots. The surface brightness at 4.85 GHz (Jy) and at 60μm (Jy/$\square'$) is used. The solid curve is an orthogonal fit to reference galaxies with a slope of 0.96 ± 0.06. The dashed lines show the "regression scissors": maximum and minimum slope (1.03 and 0.90) allowed by the data scatter.

Table 4.11: Parameters of studied galaxies related to their star formation activity

NGC	Morph. type	B-V* [mag]	mean B-V[L]	U-B** [mag]	mean U-B[L]	H I def[a]	f_{th} (Hα)	f_{th} (FIR)	SFR [$M_{\odot}yr^{-1}$] (FIR)	SFR [$M_{\odot}yr^{-1}$] (Hα)
4254	Sc	0.51	0.50±0.14	-0.03	-0.12±0.17	0.01	0.07	–	3.066	2.770
4298	Sc	0.61	0.50±0.14	–	-0.12±0.17	0.34	0.17	0.37[I]	0.675[I]	0.314
4302	Sc	0.74	0.50±0.14	–	-0.12±0.17	0.56	0.10	0.16[I]	0.675[I]	0.404
4321	SABb	0.66	0.60±0.13	-0.04	0±0.18	0.35	0.08	0.08	2.063	2.121
4388	Sb	0.58	0.61±0.16	0.15	0.03±0.20	0.69	0.02	0.04	0.871	0.386
4438	Sa	0.76	0.71±0.15	0.41	0.2±0.25	1.33	0.02	0.02	0.412	0.464
4501	Sb	0.62	0.61±0.16	0.29	0.03±0.20	0.55	0.06	0.06	1.766	1.685
4535	SBc	0.59	0.48±0.13	–	-0.12±0.15	0.19	0.12	0.07	0.811	1.278
4548	SBb	0.75	0.61±0.13	0.38	0.03±0.17	0.80	0.19	0.16	0.259	0.300
4569	SABa	0.61	0.72±0.10	0.33	0.16±0.21	1.07	0.03	0.05	0.847	0.404

* B-V corrected colour taken from LEDA database.

** U-B corrected colour taken from LEDA database.

[L] Mean value for a galaxy of a given morphological type. Calculated by us with the use of the LEDA database.

[a] Gavazzi et al. 2005, except for NGC 4321 – Chung et al. 2007.

[I] One unresolved FIR source.

Table 4.12: Magnetic field strengths and nonthermal spectral indices of studied galaxies

NGC	B_{tot} [μG]	B_{reg} [μG]	α^*_{nth}
4254	16±1.0	7.0±2.0	1
4298	8.9±2.7	2±0.9	0.91
4302	7.7±2.5	2.1±0.9	0.69
4321	11.3±3.4	2.6±1.1	0.9
4388	6.6±2.1	0.4±0.2	0.67
4438	3.9±1.3	0.6±0.3	0.53
4501	10.3±3	3.2±1.3	1
4535	8±2.4	2.5±1.1	0.9
4548	6.3±1.8	2.1±0.9	1.08
4569	8.7±2.7	1.7±0.7	0.84

Chapter 5

Summary and Conclusions

This thesis presents a sample of gas deficient and weakly star forming spiral galaxies of the Virgo Cluster. All galaxies were observed with Effelsberg radio telescope at 4.85 GHz to detect weak extended total power and polarized emission, while the radio-brightest objects were studied in more detail at 8.45 GHz or at 10.45 GHz. For almost all galaxies we used our own or archive X-ray data observed with the XMM-Newton space telescope.

The main findings of this thesis are:

- All distorted and gas deficient galaxies show moderate magnetic fields.
- Both tidal and ram-pressure effects seem to influence galaxies in a similar way, despite they act differently on both the stellar and gaseous components.
- In some cases the magnetic field in the gas deficient galaxy can be amplified to a normal level.
- X-ray observations helps to trace signs of recent distortions of gaseous disks of galaxies. In some cases they even provide direct information about the surrounding medium.
- Hot X-ray halo around M 86 seems to provide more evidence about the tidal interactions between NGC 4438 and M 86.
- Even perturbed galaxies mostly agree with the radio (4.85 GHz) – far infrared (60μm) correlation derived for non-cluster spirals. This is likely caused by the fact that external perturbations can affect both the radio and far-infrared emission by triggering enhanced star formation or truncating gaseous disks, which leads to slower star forming activity. In exceptional cases, when a galaxy hosts an active nuclei, higher

nonthermal emission from the nuclear region contributes to the radio emission, which places the galaxy above the correlation line. This can be seen for NGC 4388, NGC 4438, NGC 4501 and NGC 4579.

- NGC 4302 likely forms a physical pair with close companion NGC 4298. The asymmetries of the polarized intensity together with Hα asymmetries, H I tails, and hot gas flows visible in X-ray emission support such scenario. Between galaxies there is a region of polarized emission which, just as in the case of NGC 4038/NGC 4039, indicates amplification of magnetic field due to tidal interactions between both objects.

- Compression of the magnetic field of NGC 4535 may suggest recent interactions with the environment. This cannot be detected in any other species, as even the H I distribution is surprisingly regular. Surprisingly, in this case a strong compression does not lead to the magnetic field amplification.

- Outskirt face-on galaxy NGC 4321 lacks significant signs of perturbations. Fairly regular both polarized intensity, H I, and X-ray distribution suggest it could be relatively new member of the cluster.

Despite low resolution of this study, the "magnetic diagnostics" presented in here was proven to trace environmental effects showed by cluster galaxies interacting with each other or with hot ICM. It provides us with a very sensitive tool for examining perturbations sometimes not yet visible in other domains. When accopmanied by hot gas distribution analysis it can allow to study the evolution history of perturbed galaxies and their magnetic fields. More spiral galaxies in the Virgo Cluster observed both in radio polarimetry and X-ray emission should definitely improve our knowledge about the system as a whole, as well as provide further evidences for significant influence of the cluster environment on the properties of disk galaxies, especially their magnetic fields.

Bibliography

Beck, R., 2001, SSRv, 99, 243

Beck, R., Fletcher, A., Shukurov, A., et al., 2005, A&A, 444, 739

Beck, R., & Krause, M., 2005, AN, 326, 414

Becker, R., H., Helfand, D., J., White, R., L., et al., 2003, yCat, 8071, 0B

Becker, R., H., White, R., L., & Edwards, A., L., 1991, ApJS, 75, 1

Böhringer, H., Briel, U. G., Schwarz, et al., 1994, Nature, 368, 828

Buat, V., Boselli, A., Gavazzi, G., & Bonfanti, C., 2002, A&A, 383, 801

Carter, J., A., & Read, A., M., 2007, A&A, 464, 1155

Cayatte, V., van Gorkom, J. H., Balkowski, C., & Kotanyi, C., 1990, AJ, 100, 604

Cayatte, V., Kotanyi, C., Balkowski, C., & van Gorkom, J. H., 1994, AJ, 107, 1003

Chemin, L., Balkowski, C., Cayatte, V., et al., 2006, MNRAS, 366, 812

Chemin, L., Cayatte, V., Balkowski, C., et al., 2005, A&A, 436, 469

Chung, A., van Gorkom, J., H., Kenney, J., D., P., & Vollmer, B., 2007, A&A, 659, 115

Chyży, K., T., 2008, 482, 755

Chyży, K. T., & Beck, R., 2004, A&A, 417, 541

Chyży, K., T., Bomans, D., J., Krause, M., et al., 2007, A&A, 462, 933

Chyży, K., T., Ehle, M., & Beck, R., 2007, A&A, 474, 415

Chyży, K., T., Knapik, J., Bomans, D., J., et al., 2003, A&A, 405, 513

Chyży, K., T., Soida, M., Bomans, D. J., et al., 2006, A&A, 447,465

Chyży, K., T., Urbanik, M., Soida, M., & Beck, R., 2002, Ap&SS, 281, 409

Chyży, K., T., Weżgowiec, M., Beck, R., & Bomans, D., J., in prep.

Combes, F., Dupraz, C., Casoli, F., & Pagani, L., 1988, A&A Let., 203, L9

Condon, J. J., 1987, ApJS, 65, 485

Condon, J. J., Cotton, W. D., Greisen, E., W., et al., 1998, AJ, 115, 1693

Emerson, D. T., & Gräve, R., 1988, A&A, 190, 353

Emerson, D. T., Klein, U., & Haslam, C. G. T., 1979, A&A, 76, 92

Gabriel, C., Denby, M., Fyfe, D., J., et al., 2004, ASPC, 314, 759

Gallimore, J., F., Axon, D., J., O'Dea, C. P., et al., 2006, AJ, 132, 546

Gavazzi, G., 1998, in Untangling Coma Berenices: A New Vision of an Old Cluster, eds. A. Mazure, F. Casoli, F. Durret, D. Gerbal, Word Scientific Publishing Co Pte Ltd, p 73.

Gavazzi, G., Boselli, A., van Driel, W., & O'Neil, K., 2005, A&A, 429, 439

Gavazzi, G., Boselli, A., Pedotti, P., et al., 2003, Hα surface photometry in Virgo, VizieR On-line Data Data Catalog: J/A+A/396/449

Gioia, I. M., Gregorini, L., & Klein, U., 1982, A&A, 116, 164

Gunn, J. E. & Gott, J. R., 1972, ApJ, 176, 1

Haslam, C. G. T., 1974, A&A Suppl., 15, 333

Heald, G., H., Rand, R., J., Benjamin., R., A., & Bershady, M., A., 2007, ApJ, 663, 933

Helou, G., & Walker, D., W.,1985, IRAS Small Scale Structure Catalog, Ver 1.00 Vizier Online Data Catalog: VII/73

Hummel, E., & Saikia, D., J., 1991, A&A, 249, 43

Jansen, F., Lumb, D., Altieri, B., et al., 2001, A&A, 365, 1

Kaastra, J., S., 1992, An X-Ray Spectral Code for Optically Thin Plasmas (Internal SRON-Leiden Report, updated version 2.0)

Kalberla, P., M., W., Burton, W., B., Hartmann D., et al., A&A, 440, 775

Kenney, J. D. P., Rubin, V. C., Planesas, P., & Young, J. S., 1995, ApJ, 438, 135

Kenney, J., D., P., Tal, T., Crowl., H., H., et al., 2008, ApJL, 687, 69

Kennicutt, R., C., Jr., 1998, ApJ, 498, 541

Kennicutt, R., C., Jr., & Kent, S., M., 1983, AJ, 88, 1094

Knapen, J., N., Cepa, J., Beckman, J., E., et al., 1993, ApJ, 416, 563

Koopman, R., A., & Kenney, J., D., P., 2004, ApJ, 613, 866

Koopman, R., A., Kenney, J., D., P., & Young, J., 2001, ApJS, 135, 125

Kotanyi, C., G., & Ekers, R., D., 1983, A&A, 122, 267

Machacek, M., E., Jones, C., & Forman, W., R., 2004, ApJ, 610, 183

Mewe, R., Gronenschild, E., H., B., M., & van den Oord, G., H., J., 1985, A&AS, 62, 197

Minchin, R., Davies, J., Disney, M., et al., ApJ, 670, 1056

Morsi, H. W., & Reich, W., 1986, A&A, 163, 313

Nagar, N., M., Falcke, H., & Wilson, A., S., 2005, A&A, 435, 521

Niklas, S., Klein, U., & Wielebinski, R., 1995, A&A, 293, 56

Niklas, S., Klein, U., & Wielebinski, R., 1997, A&A, 322, 19

Onodera, S., Koda, J., Sofue, Y., & Kohno, K., 2004, PASJ, 56, 439

Otmianowska-Mazur, K., & Vollmer, B., 2003, A&A, 402, 879

Paturel, G., Petit, C., Prugniel, P., et al., 2003, A&A, 412, 45

Phookun, B., Vogel, S.,N., & Mundy, L.,G., 1993, ApJ, 418, 113

Reddy, N., A., & Yun, M., S., 2004, ApJ, 600, 695

Schmidt, A., Wongsowijoto, A., Lochner, O., et al., 1993, MPIfR Technical Report No. 73, MPIfR, Bonn

Shibata, R., Matsushita, K., Yamasaki, N., Y., et al., 2001, ApJ, 549, 228

Soida, M., Otmianowska-Mazur, K., Chyży, K., T., & Vollmer, B., 2006, A&A, 458, 727

Soida, M., Urbanik, M., & Beck, R., 1996, A&A, 312, 409

Soida, M., Urbanik, M., Beck, R., et al., 2001, A&A, 378, 40

Soria, R., & Wong, D., S., 2006, MNRAS, 372, 1531

Strüder, L., Briel, U., Dennerl., K., et al., 2001, A&A, 365, 18

Toomre, A., & Toomre, J., 1972, ApJ, 178, 623

Tschöke, D., Bomans, D., J., Hensler, G., & Junkes, N., 2001, A&A, 380, 40

Turner, M., J., L., Abbey, A., Arnaud, M., et al., 2001, A&A, 365, 27

Urbanik, M. in The Magnetized Plasma In Galaxy Evolution, eds.: Chyży, K. T., Otmianowska-Mazur, K., Soida, M., Dettmar, R-J., p. 201

Urbanik, M., Klein, U., & Gräve, R., 1986, A&A, 166, 107

Vollmer, B., Balkowski, C., Cayatte, V., et al., 2004, A&A, 419, 35

Vollmer, B., Braine, J., Combes, F., & Sofue, Y., 2005, A&A, 441, 473

Vollmer, B., Cayatte, V., Balkowski, C., & Duschl, W. J., 2001, ApJ, 561, 708

Vollmer, B., Cayatte, V., Boselli, A., et al., 1999, A&A, 349, 411

Vollmer, B., Soida, M., Beck, R., et al., 2007, A&A, 464L, 37

Vollmer, B., Soida, M., Chung, A., et al., 2008, A&A, 483, 89

Weiler, K., W., van der Hulst, J., M., Sramek, R., A., & Panagia, N., 1980, BAAS, 12, 752

Weżgowiec, M., Urbanik, M., Vollmer, B., et al., A&A, 471, 93

Wong, T., & Blitz, L., 2002, ApJ, 569, 157

Yoshida, M., Ohyama, Y., Iye, M., et al., 2004, AJ, 127, 90